Contents lists available at ScienceDirect

Journal of Structural Geology

journal homepage: http://ees.elsevier.com

Intrusion fracturing and quartz sand-rich injections in thrust-related fault rocks within the basal shear zone of the Esla Nappe (Cantabrian Zone, NW Iberia)

Manuel Ignacio de Paz-Álvarez*, Sergio Llana-Fúnez, Juan Luis Alonso

Departamento de Geología, Universidad de Oviedo, C/ Jesús Arias de Velasco S/n, 33005, Oviedo, Spain

ARTICLE INFO

Keywords
Sand injection
Thrust-related deformation
Fault rocks
Fluid overpressure
Cantabrian zone

ABSTRACT

The Esla Nappe, located in the Cantabrian Zone (Variscan Orogen, NW Iberia), has an estimated 19 km displacement to the NE accommodated in a thin (<2–3 m) shear zone (ENSZ) at least 4 km depth. Fault-rock assemblages record different deformation processes operating in the hangingwall and footwall. While the hangingwall was largely deformed through cataclastic flow localised in a <50 cm band, hangingwall-footwall intervening ultracataclasites and footwall lithologies preserve evidence for an interplay of cataclastic flow and pressure solution. Final hydrofracturing and calcite vein precipitation has contributed to the vertical dilation of the fault rock assemblages.In the late stages of emplacement, the ENSZ was breached through intrusion fracturing and associated clastic sills and dykes injected along re-opened previous discontinuities and anisotropies. Together, they conform an interconnected network of quartz sand-rich lithosomes reaching structural heights of 20 m over the ENSZ. Injections are formed by a mixture of injected quartz grains and host-derived fragments. Dyke orientations suggest that the injection process occurred under large fluid overpressure conditions exceeding lithostatic values in the footwall. Fluid overpressure may have been caused by progressive fluid accumulation beneath a low-permeability ultracataclasite layer at the base of the nappe. Breaching through the shear zone was favoured by a change in the stress regime following the Esla Nappe emplacement.

1. Introduction

The mobilization of sand and its injection along sills and dykes is a common process in unconsolidated sediments at depths usually <1500 m (Jolly and Lonergan, 2002; Jonk, 2010; Hurst et al., 2011). The process requires the development of fluid overpressure exceeding a critical threshold, hydrofracturing or reopening of discontinuities, sand liquefaction and fluidization (Maltman, 1994; Jolly and Lonergan, 2002; Hurst et al., 2011). Fluid overpressure within the parent sandstone body is required to (i) overcome the minimum principal stress and the tensile strength of the overlying rocks if a new fracture is to be formed and injected (Jolly and Lonergan, 2002), or to (ii) overcome the normal stress acting across a discontinuity and the tensile strength of the material inside if it is to be reopened and injected (Delaney et al., 1986; Jolly and Sanderson, 1997).

Fluid pressure increases have been attributed to several causes that operate on varied geological timescales, such as disequilibrium compaction (Osborne and Swarbrick, 1997), rapid loading (Jonk, 2010), lateral fluid transfer (Mann and Mackenzie, 1990), diagenesis (Helset et al., 2002), dehydration reactions (Murrell and Ismail, 1976; Llana-Fúnez et al., 2012), fluid temperature and/or pressure increase (Bethke, 1985), fluid influx (Brooke et al., 1995; Jonk, 2010), tectonic compressive stresses (Osborne and Swarbrick, 1997), seismicity-induced liquefaction (Jolly and Lonergan, 2002), or thermal pressurization (Andrews, 2002; De Paola et al., 2011).

Many of the injectite complexes described in the literature are located in extensional sedimentary basins, where the maximum compressive stress is vertical (Duranti and Hurst, 2004; Duranti, 2007). There, injections tend to be normal to the minimum principal stress and vertical (Jolly and Lonergan, 2002). However, in contractional environments, sand injection is problematic due to the unfavourable orientation of the principal stresses, as the minimum principal stress is equivalent to the overburden (Palladino et al., 2016). Injections are expected to intrude along subhorizontal discontinuities, and that requires a partial lifting of the overburden driven by near-lithostatic fluid pressures (DiTullio and Byrne, 1990; Vigorito and Hurst, 2010). Nonetheless, a few contributions have dealt with injection complexes in close relation with contractional structures (*e.g.* Taylor, 1982; Winslow, 1983; DiTullio and Byrne, 1990; Phillips and Alsop, 2000; Palladino et al., 2016).

A key factor in the formation of clastic dykes and sills is the degree of lithification of the sandstone parent unit from which they are derived. The process of sand liquefaction, fluidization and injection neces-

* Corresponding author.
E-mail addresses: midepaz@geol.uniovi.es (M.I. de Paz-Álvarez); llanasergio@uniovi.es (S. Llana-Fúnez); jlalonso@geol.uniovi.es (J.L. Alonso)

https://doi.org/10.1016/j.jsg.2020.104230
Received 8 June 2020; Received in revised form 1 November 2020; Accepted 4 November 2020
Available online xxx
0191-8141/

sarily requires a source of unconsolidated granular material (Maltman, 1994). Therefore, a relatively short time span between sediment deposition and injection is usually invoked (<5 Myr, Duranti and Hurst, 2004; <10 Myr, Vigorito and Hurst, 2010). However, some studies have argued for the possibility for pockets of sediment to remain overpressured and unlithified prior to injection for large periods of time (120 Myr; Phillips and Alsop, 2000).

The host lithology where intrusion fracturing occurs is usually considered sufficiently cohesive to be able to fracture, but rarely a completely lithified competent unit (*e.g.* Labaume, 1987; DiTullio and Byrne, 1990; Cosgrove, 1995, Duranti and Hurst, 2004). Only a few contributions have dealt with the intrusion fracturing and injection in consolidated rocks (*e.g.* Chi et al., 2012). In this contribution we adopt the term intrusion fracturing *sensu* Mandl (1999), defined as fracturing induced in a rock mass by externally derived, and not internally hosted, overpressured fluids.

The Esla Nappe (EN) in the foreland-fold-and-thrust belt of the Variscan Orogen of Iberia (Cantabrian Zone), hosts an injection complex at its basal shear zone (Arboleya et al., 1999), which is extraordinary for several reasons: (i) it was formed in a contractional setting during orogenesis; (ii) it mobilized large volumes of granular material; (iii) it involved the fluidization of sandstones deposited 65 Myr prior to their injection into completely lithified competent overlying limestones; and (iv) it was emplaced with a minimum overburden of *ca.* 110 MPa (*ca.* 4300 m). This contribution aims to expand previous research on the deformation associated to the EN basal shear zone (Arboleya, 1989; Arboleya et al., 1999). New field and microstructural observations have led to a reappraisal of the deformation mechanisms and processes operating during the movement and emplacement of the Esla Nappe, and in particular, of the timing and causes for the generation of the injectite complex intruded at its base.

2. Regional geology

2.1. Geological setting

The Cantabrian Zone constitutes the external foreland-fold-and-thrust belt of the Variscan Orogen in the NW Iberian Massif (Fig. 1A). Deformation was accomplished through the emplacement of several thrust units with associated folds during the Pennsylvanian (Pérez-Estaún et al., 1988). The E–W trending León Thrust, a major out-of-sequence breaching structure, duplicated several of the palaeogeographic domains around the Moscovian-Stephanian boundary (Alonso et al., 2009) (Fig. 1A). In the late stages of the Variscan orogeny, during the Stephanian, a mega-arcuate structure was formed, with the orogen trend describing a 180° rotation with Cantabrian Zone located at its core (*e.g.* Julivert and Marcos 1973). Whether the arc was formed by buckling of a previously linear orogen (Gutiérrez-Alonso et al., 2004) or bending associated to the indentation of an irregular continent (*e.g.* Matte 1986; Llana-Fúnez and Marcos 2007), the arc closure in the Cantabrian Zone led to the tightening of nappe-related folds, the reorientation of the frontal and lateral structures, and the steepening and overturning of thrusts (Alonso, 1987b, 1989). Recent N–S Alpine convergence further contributed to fold tightening and reactivation of favourably oriented earlier faults (*e.g.* Alonso et al. 1996).

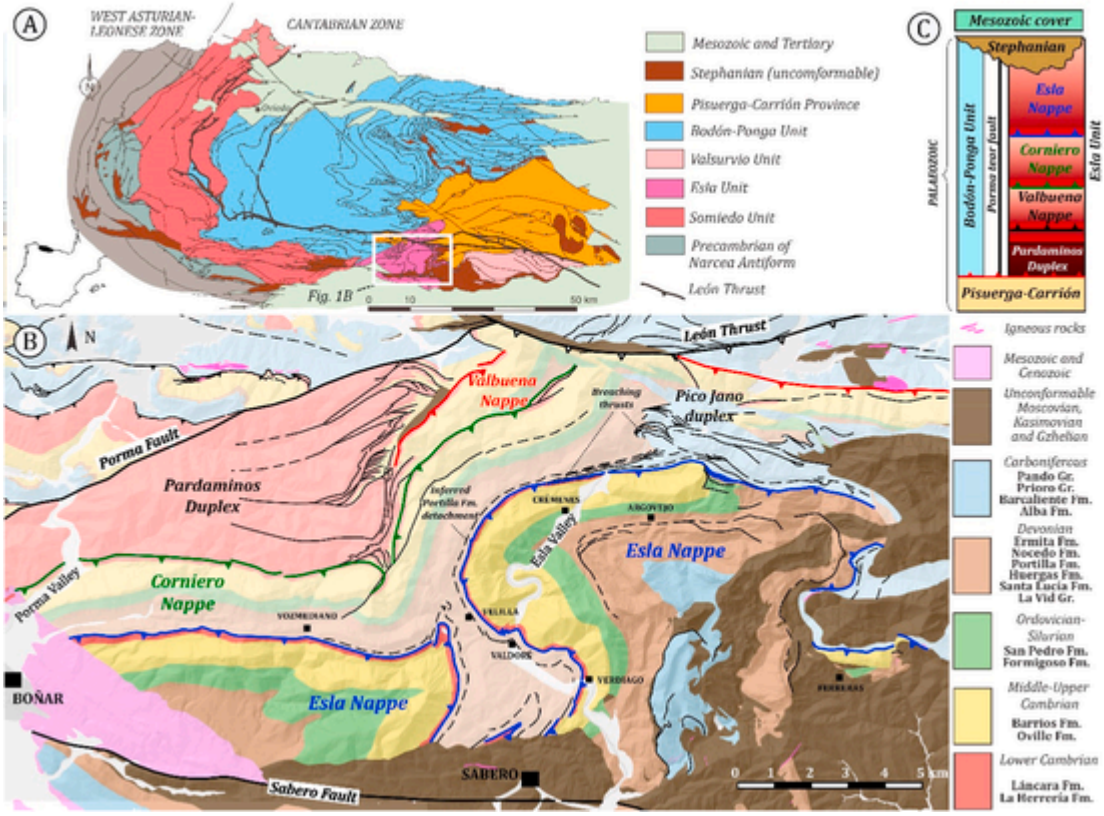

Fig. 1. (A) Geological map of the Cantabrian Zone (modified from Alonso et al., 2009). (B) Simplified geological map of the Esla Unit, modified from Merino-Tomé et al. (2014). Black thin lines represent thrust faults: triangle symbols have been omitted for clarity. Esla Nappe colours have been highlighted. Note the presence of a detachment at the base of the Portilla Fm. (C) Tectonostratigraphic chart after Alonso (1987b). (For interpretation of the references to colour in this figure legend, the reader is referred to the Web version of this article.)

2.2. The Esla Nappe

The Esla Nappe is the uppermost nappe in the Esla Unit, located in the SE of the Cantabrian Zone (Fig. 1B; Alonso, 1987b). Its stratigraphy and structure have been the focus of numerous investigations (Comte, 1959; de Sitter, 1959; Rupke, 1965; Arboleya, 1981; Alonso, 1987a, 1987b, 1989). An accumulated displacement of *ca.* 19 km has been estimated on the basis of the retrodeformation of geological balanced cross-sections (Alonso, 1987b). A transport sense towards the NE was proposed by de Sitter (1959), Arboleya (1981) and Alonso (1987b) on the basis of the direction in which the thrust cuts up section, fault-rock-related structures, the trend of major thrust-related folds, and cut-off lines of formations truncated by the thrust ramp. A similar transport sense is supported by our own data of small-scale structures measured at the base of the Esla Nappe (Fig. 2). Nappe emplacement took place during the Moscovian (Fig. 3; Alonso, 1987a; Oliveira et al., 2019). The basal thrust of the *ca.* 4300 m-thick Esla Nappe is characterised by a large hangingwall flat developed in the Lower Cambrian Láncara Formation, and two large footwall flats developed at the top of the Devonian Huergas Fm., to the West, and of the Devonian Portilla and Ermita fms., to the East (Fig. 1B; Rupke, 1965; Arboleya, 1981). In its SE margin, the nappe rests close to the top of the Devonian Nocedo Fm., preserved below an Upper Devonian unconformity. Towards the NE, the basal thrust surface climbs up section in both the footwall and hangingwall, until reaching the Bashkirian Prioro Gr. and the Devonian Huergas Fm., respectively. The Pico Jano duplex accumulated at the frontal part of the system *ca.* 10 km of displacement at the rear of the Esla Nappe, once the original footwall ramp was breached and a new detachment horizon developed at the base of the Alba Fm. ahead of the branch line (Alonso, 1987b). In the late stages of emplacement, the Esla footwall ramp was again

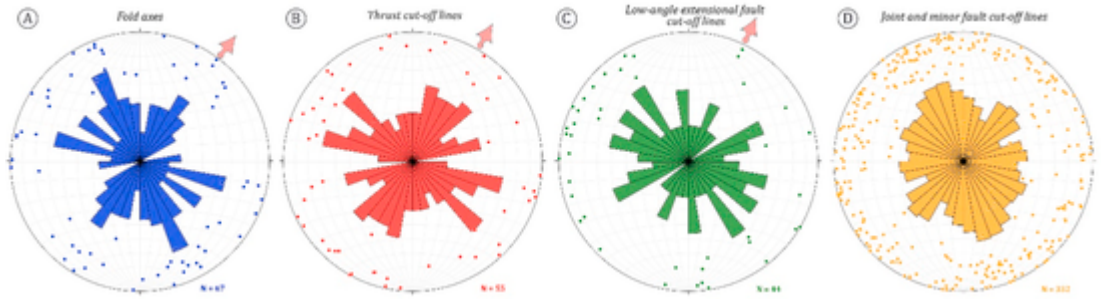

Fig. 2. Lower-hemisphere equal-area stereoplots displaying the restored orientations of structures used as kinematic indicators for the emplacement of the Esla Nappe. They are small-scale structures located at the ENSZ or in close proximity to it: fold axes (A), thrust cut-off lines (B), cut-off lines of minor Riedel-like low angle extensional faults (C), joints and minor high angle faults (D). Arrows indicate the transport direction for each plot. Note that rose diagrams are constructed so that the number of data is proportional to the area of the wedges, not to their length.

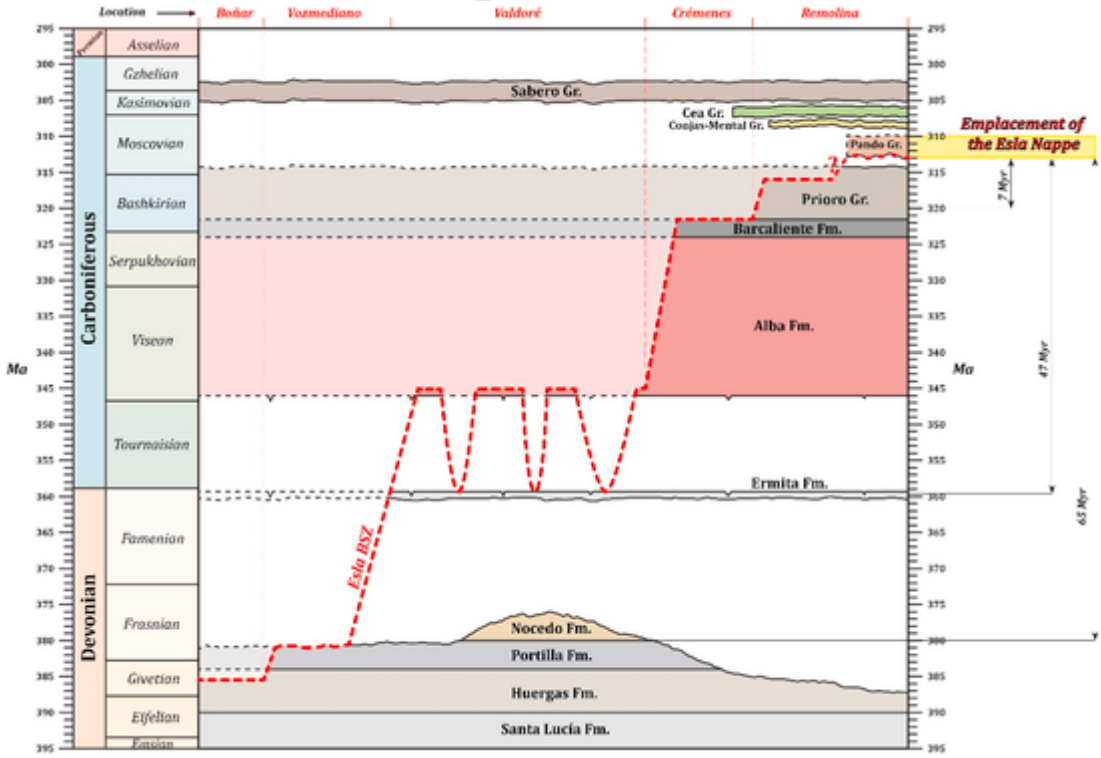

Fig. 3. Synthetic chronostratigraphic chart of the footwall to the ENSZ (Corniero Nappe). Note the two main sedimentary hiatuses at the base of the Ermita and Alba formations. The position of the EBSZ in different locations is shown with a red dashed line: note the two main footwall flats atop the Huergas-Portilla fms. and Alba-Ermita fms. The emplacement of the Esla Nappe is temporally referred to the deposition of the Nocedo Fm., Ermita Fm., and Prioro Gr. Formation ages derived from Rupke (1965), van Adrichem Boogaert (1967), Reijers (1972), van Loevezijn (1986), Alonso (1987a), Oliveira et al. (2019). Note that the vertical scale is referred to chronostratigraphy, and not to formation thicknesses. (For interpretation of the references to colour in this figure legend, the reader is referred to the Web version of this article.)

broken and displacement was transferred to the base of the underlying Portilla Fm., as inferred from the breaching of the Pico Jano duplex floor thrust (Fig. 1B; a detailed description can be found in Alonso, 1987b). The nappe is unconformably overlain by late Moscovian and Kasimovian synorogenic deposits towards the East (Fig. 1B; Rupke, 1965; Alonso, 1987a).

2.3. Fault rocks at the base of the Esla Nappe

Fault rocks associated to the basal shear zone of the Esla Nappe (ENSZ) were studied by Arboleya (1983; 1989) and Arboleya et al. (1999), who identified breccias with a quartz-rich matrix in the hangingwall, proto-, meso- and ultracataclasites, often with a penetrative planar fabric, with variable quartz content in the footwall, and small quartz-filled injections into the hangingwall, some 10 cm long and 4 cm thick. The injection of these exotic quartz grains was attributed to hydraulic fracturing following events of high pore fluid pressure, which carried quartz grains sampled from the Upper Devonian sandstones of the footwall (van der Meer Mohr, 1969; Arboleya, 1989). The finding of considerably larger sand dykes, several meters long and injected at a maximum structural height of 20 m from the base of the nappe into the hangingwall, together with the possibility of updating the microstructural techniques used for the study of its fault rocks, have motivated this new study on the rocks and structures at the base of the Esla Nappe.

3. Methods

Fieldwork was conducted along the ENSZ in order to produce a detailed map and collect samples of the fault rocks and structures along the base of the unit. Structural measurements were plotted in a lower hemisphere equal-area (Schmidt) stereographical projection and rotated to their restored orientation with the aid of Stereonet software (Allmendinger et al., 2012). The traditional rotation method of bringing fold axes to horizontal and subsequently their limbs (tenHaaf, 1959) is not valid in the Esla area, as most of the deformation subsequent to nappe emplacement occurred through the tightening and reorientation of previously plunging folds. The area has been subdivided in sectors that experienced different deformation paths based on the structural evolution of the Esla Nappe (Alonso, 1987b), and their data rotated accordingly. Polished thin sections produced at the University of Oviedo were studied under transmitted and reflected light in optical microscopes, and with a JEOL 6610LV Scanning Electron Microscope (SEM) with an associated Energy-Dispersive X-ray analyser (EDX).

X-ray diffraction (XRD) measurements were carried out in unoriented powdered samples with a PANalytical X'Pert Pro diffractometer with a X'Celerator detector. Radiation source was the Cu K-α at 1.54056 Å, operating at 45 kV and 40 mA. Data was analysed with PANalytical X'Pert Highscore Plus software, used with ICDD powder diffraction file database PDF-4. Basic Rietveld refinement of the diffraction pattern has allowed a semi-quantitative determination of the phases present in the samples.

Grain size distributions of fault rocks were studied from thin section by optical and electron microscopy. Individual grains in photomicrographs were drawn by hand to produce bitmaps of the samples and analysed with ImageJ software. Fragment equivalent diameter ($\varnothing_{eq}$), defined as the diameter of a circle of the same area as the grain section ($\varnothing_{eq} = 2\sqrt{Area/\pi}$) was calculated and plotted against N on a log-log graph, where N equals the number of grains with sizes larger than $\varnothing_{eq}$. Linear trends observed in this representation can be fit through a power law in the form $N = C\,\varnothing_{eq}^{-D}$, where D is the two-dimensional fractal dimension (D_{2D}) (Blenkinsop, 1991). D_{3D} can be calculated adding one to D_{2D} (Sammis et al., 1987). All D values expressed in this study are given as D_{3D}.

4. Stratigraphy

The stratigraphy of the Esla Nappe and its relative autochthon, the Corniero Nappe, has been thoroughly investigated previously (*e.g.* Rupke, 1965). It is formed by an almost complete Palaeozoic sedimentary succession characterised by alternations of carbonate formations, largely limestones, and siliciclastic units consisting of sandstones, quartzarenites and shales. In this section a brief outline of the lithostratigraphic formations investigated in this contribution which are involved in the deformation of the Esla Nappe is provided. A more comprehensive description can be found in the references in the caption of Fig. 3. The age of the formations and their relative position with respect to the ENSZ is provided in Fig. 3.

4.1. Footwall formations of the Corniero Nappe

The Huergas Formation is constituted by yellow-reddish sandstones and characteristically brown shales. Sandstones typically display a characteristic patchy ferruginous cement: in other areas cement is formed by both quartz and minor calcite. Its thickness varies between *ca.* 70 m in the W sector and 200 in the E sector.

The Portilla Formation is conformed by limestones with different textures, including mudstones, wackestones, packstones, boundstones, floatstones as well as marls, usually with a light-grey colour. Grain components are bioclastic, and include crinoids, brachiopods, stromatoporoids and corals. Its thickness varies between 60 m in the W sector and 120 m in the E sector.

The Nocedo Formation is formed by light-yellow and red-stained fine-grained quartz-arenites. Its maximum thickness is 60 m in the SE sector, and progressively thins towards the West due to Upper Devonian erosion. Light-coloured sandstones are locally carbonate-cemented and porous, whereas the upper red sandstones are often massive, without preserved sedimentary structures.

The Ermita Formation is found unconformably on top of the Nocedo and Portilla fms. along a 1°–3°-dipping unconformity angle. It is formed by 2–6 m-thick white to dark-red quartz-bearing sandy bioclastic grainstones with local glauconite, and display frequent cross-lamination.

The Alba Formation is paraconformable, and restricted to local areas of the footwall, with a variable thickness of 2–5 m. It is formed by dark red marls with intercalated nodular pink mudstones and wackestones with scarce skeletal content.

The Barcaliente Formation is formed by dark and well-bedded micritic limestones, locally with frequent mm-scale laminations. Its thickness is difficult to establish in the area due to thrust duplications, but is in the order of 250 m.

The Prioro Group comprises well-bedded dark limestones and marls, shales, sandstones and chaotic block-in-matrix deposits.

4.2. Hangingwall formations of the Esla Nappe

The investigated formations of the hangingwall were the carbonates of the Láncara and Santa Lucía fms. Other formations present in the hangingwall ramp include the Oville, Barrios, Formigoso, San Pedro, La Vid and Huergas fms., but the ENSZ does not crop out when they are at the base of the hangingwall.

The Cambrian Láncara Fm. in contact with the ENSZ is formed by light-grey micritic limestones with frequent calcite-filled birdseyes. Locally, camel-coloured dolomicrites with local development of algal laminations are located instead at the base.

The Devonian Santa Lucía Formation is formed by limestones displaying a wide range of facies, spanning from wackestones to grainstones, with local development of reefal bioconstructions.

5. Fault rocks

Fault rocks derived from both footwall and hangingwall lithologies are found in the ENSZ forming an assemblage varying in thickness between 20 cm and 8 m. They vary among different zones within the nappe. A semi-quantitative estimation of their mineral phases is shown in Table 1.

Table 1
Summary of the characteristics of the described fault rocks of the ENSZ, as well as of the siliciclastic formations from the uppermost footwall. Grain size distributions of the samples are shown in Fig. 7. Semi-quantitative modal abundance (%) of mineral phases determined from XRD measurements.

Rock	Phase	%	Description	Analysed	Sample	Precursor formation	Distribution	D_{3D} value	Matrix (%) (<100 μm)	D_{3D} mean	D_{3D} interpretation
LD-BC Limestone and dolostone breccias and cataclasites	Cal	7	Dolostone and limestone fragments are angular and embedded in a matrix of the same composition.	Carbonate	VOZL1	Láncara	–	–	22	2.99	These values, in excess of the predicted value for the constrained comminution model (Sammis et al., 1987), are the result of scale-dependant comminution processes, such as large particle abrasion and selective breakage.
					FERL2	Láncara	Power law	3.05	70		
	Dol	90			VOZL42	Láncara	Power law	3.06	76		
	Qz	3			VOZL39	Láncara	Power law	2.87	94		
	Sme-Illi	0			OCES1	Santa Lucía	Power law	2.98	78		
LQz-U Quartz-bearing limestone ultracataclasites	Cal	72	Limestone fragments are smooth and sub-rounded, generally formed by fine-grained micrite with abundant authigenic quartz crystals. Quartz fragments are angular and generally smaller than 50 μm. Both are embedded in a very fine-grained matrix formed by calcite, quartz, clay minerals, apatite, Fe–Ti oxides and zircon.	Carbonate	VONL12	Láncara	Power law	3.70	98	3.52	These values, in excess of the predicted value for the constrained comminution model (Sammis et al., 1987) and for the operation of self-similar deformation processes (Heilbronner and Keulen, 2006), are the result of selective comminution in relation to shear localisation.
					VELL6C	Láncara–Ermita	Power law	3.30	96		
	Dol	3			SAHL10	Láncara–Ermita	Power law	3.56	68		
			Quartz	VONL12		Huergas	Power law	3.23		3.20	
	Qz	19			VELL6C	Nocedo–Ermita	Power law	3.16			
			SAHL10	Nocedo–Ermita			Power law	3.38			
	Sme-Illi	6			VELL31	Nocedo–Ermita	Power law	3.02			

Rock	Phase	%	Description	Analysed	Sample	Precursor formation	Distribution	D_{3D} value	Matrix (%) (<100 μm)	D_{3D} mean	D_{3D} interpretation
QzLD-B Quartz-rich limestone and dolostone breccias	Cal	42	Limestone fragments are angular, texturally varied and corroded. Quartz grains are sub-rounded and well sorted, with their boundaries variably corroded. They are cemented by calcite, which is locally fragmented, in which case the resulting porosity is filled with clay minerals. In these areas, quartz grains have also been fractured.	Carbonate	VERL10	Láncara	Power law	3.06	–	3.06	Intrusion brecciation of pre-fractured Láncara Fm.
	Dol	18		Quartz	VELL29	Nocedo–Ermita	Partial power law	2.48	59 (including Qz, considered matrix)	2.47	With the exception of the simple-shear fracture with developed cataclasis (VELL6F_cat, excluded from mean), the values are consistent with tensile fracturing (Blenkinsop, 1991). In unfractured areas, the log-normal distribution is inherited from the parent source of the injections.
			VELL6F		Nocedo–Ermita		Partial power law	2.46			
	Qz	36			VELL6F_cat	Nocedo–Ermita	Power law	2.73			
	Sme-Illi	4			VELL4	Nocedo–Ermita	Log-normal	–			

Rock	Phase	%	Description	Analysed	Sample	Precursor formation	Distribution	D_{3D} value	Matrix (%) (<100 μm)	D_{3D} mean	D_{3D} interpretation
Dykes and sills Quartz-rich injections with limestone fragments	Cal	43	Quartz grains are texturally very similar to those in QzLD-B, as are the limestone fragments. The main difference between the two rocks is the lower limestone content in the dykes and sills. Locally, crosscutting dykes are present, though their textural similarity hinders their macroscopic identification.	Quartz	ARGB6	Prioro	Partial power law	2.35	–	2.43	In fractured areas, the values are consistent with tensile fracturing (Blenkinsop, 1991). In unfractured areas, the log-normal distribution is inherited from the parent source of the injections.
	Dol	4			OCES5	Prioro	Power law	–			
	Qz	51			VERL7	Nocedo–Ermita	Partial power law	2.50			
	Sme-Illi	2			VOZL9	Nocedo–Ermita	Power law	–			
Siliciclastic formations	Cal	15	Siliciclastic formations of Devonian and Carboniferous age contain quartz grains which are similar in size and shape to those within the injections. Quartz grains are also locally corroded by their calcite cement.	Quartz	OCES11	Prioro	Log-normal	–	–	–	The log-normal distribution results from the original sedimentary particle distribution, and is unrelated to deformation.
	Dol	0			Ermita	Ermita	Log-normal	–			
	Qz	79			VERE2	Nocedo	Log-normal	–			
	Sme-Illi	6			VONH1	Huergas	Log-normal	–			

5.1. Fault rocks located West of Vozmediano (rear of the Esla Nappe)

In this area the Esla Nappe displays at its base dolomicrites of the Lower Member of the Láncara Fm., and rests on footwall lithologies either formed by sandstones and shales of the Huergas Fm. or by limestones of the Portilla Fm. (Figs. 1B and 3).

Quartz cataclasites in the footwall are restricted to <10 cm, usually <1 cm (Figs. 4A, 5A and 6A). They are formed by crushed quartz grains with scarce clay matrix between fragments. Their planar fabric is caused by the presence of numerous thin (<20 μm) extension calcite veins with an anastomosing pattern which have locally accomplished over 50% vertical dilation.

Limestone and dolostones in the hangingwall have been variably deformed in a usually <50 cm-thick interval. Fine-grained ultracataclasites with scarce quartz and dolostone fragments are locally developed, but are not laterally continuous at the outcrop scale. Cataclasites (LD-BC, limestone-dolostone breccias and cataclasites) are formed by angular fragments of micritic limestones or dolostones embedded in a fine-grained matrix of the same composition (Figs. 4A and 5A). Fragments preserve sedimentary facies from the Lower Member of the Láncara Fm., from which they have developed through progressive fragmentation and disaggregation. Where the nappe rests on the Huergas Fm., scarce sub-rounded quartz sedimentary grains are present between dolostone fragments (Fig. 5A). Fragment-size cumulative plots (FSCP) suggest a power-law distribution of $\varnothing_{eq}$ with a D_{3D} in the order of 2.87–3.06 in the cataclasites, and 3.70 in the ultracataclasites (Table 1 and Fig. 7A; VONL12 in Fig. 7B). Cataclasites grade upwards into crackled breccias and fragmented host rock.

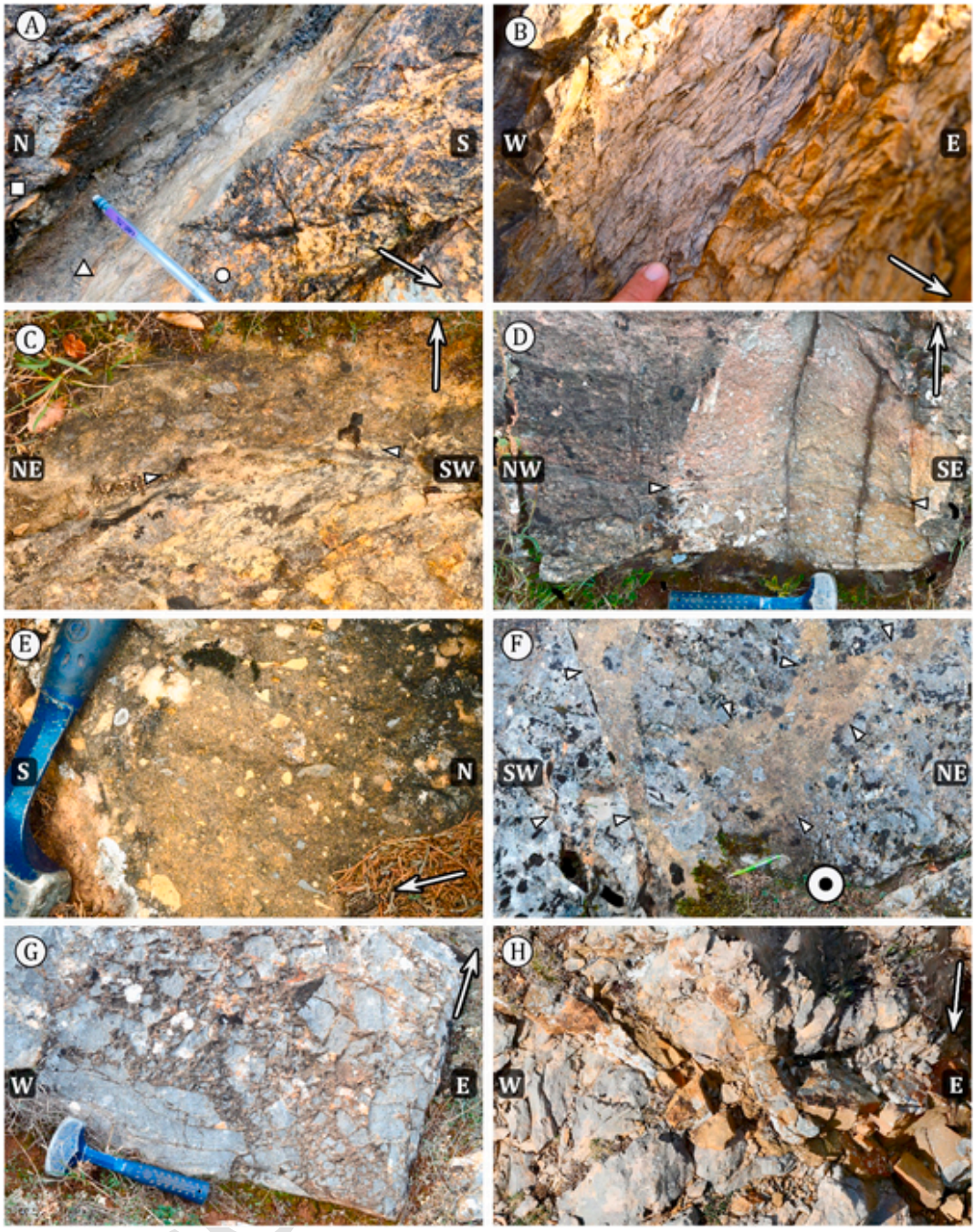

Fig. 4. Field photographs of the fault rocks located in the ENSZ. Arrows indicate the top of the succession. Locations are indicated in Fig. 10C and 11. (A) Láncara-derived cataclasites (right, circle) and Huergas sandstones (left, square), separated by a thin layer of quartz cataclasites with a penetrative planar fabric (triangle). Location NE of Voznuevo. (B) Fine-grained LQz-U with a penetrative planar fabric. Colour differences are related to weathering. Location N of Verdiago. (C) Sharp contact between LQz-U (below, light) and Láncara-derived QzLD-B (above, dark), marked with white triangles. Location SW of Velilla. Height of picture frame is 20 cm. (D) Láncara-derived QzLD-B cut by a thin subhorizontal quartz-rich sill (marked with triangles). Location NE of Velilla. (E) QzLD-B with Láncara Fm.-derived dolomicrite fragments in an out-of-sequence thrust placing Ermita Fm. over Alba Fm. Location N of Crémenes. (F) Interconnected quartz-rich dykes (highlighted with white triangles) with detached host fragments seen on a bedding surface of the Láncara Fm. Location SW of Velilla. (G) Irregularly shaped quartz-rich dyke with abundant Láncara Fm. host fragments. Note the quartz-sand filled jigsaw fractures at the boundaries. Location N of Valdoré. (H) Bifurcating quartz-sand rich dykes crosscutting Santa Lucía Fm. limestones. Location NE of Argovejo. Height of picture frame is approximately 65 cm. (For interpretation of the references to colour in this figure legend, the reader is referred to the Web version of this article.)

5.2. Fault rocks located between Vozmediano and Argovejo (central portion of the Esla Nappe)

In this area, the base of the Esla Nappe is mostly formed by the limestones of the Lower Member of the Láncara Fm., whereas the footwall displays either grainstones of the Portilla and Ermita fms. or a thin veneer of the mudstones of the Alba Fm. Quartzarenites of the Nocedo Fm. are present in a large part of the area very close to the ENSZ (<5–10 m) most notably in the Valdoré tectonic semi-window (Figs. 1B and 3).

Ermita and Portilla-derived limestone cataclasites in the footwall are formed by large (<2 mm) elongated fragments of monocrystalline echinoid ossicles and local quartz grains embedded in a fine-grained

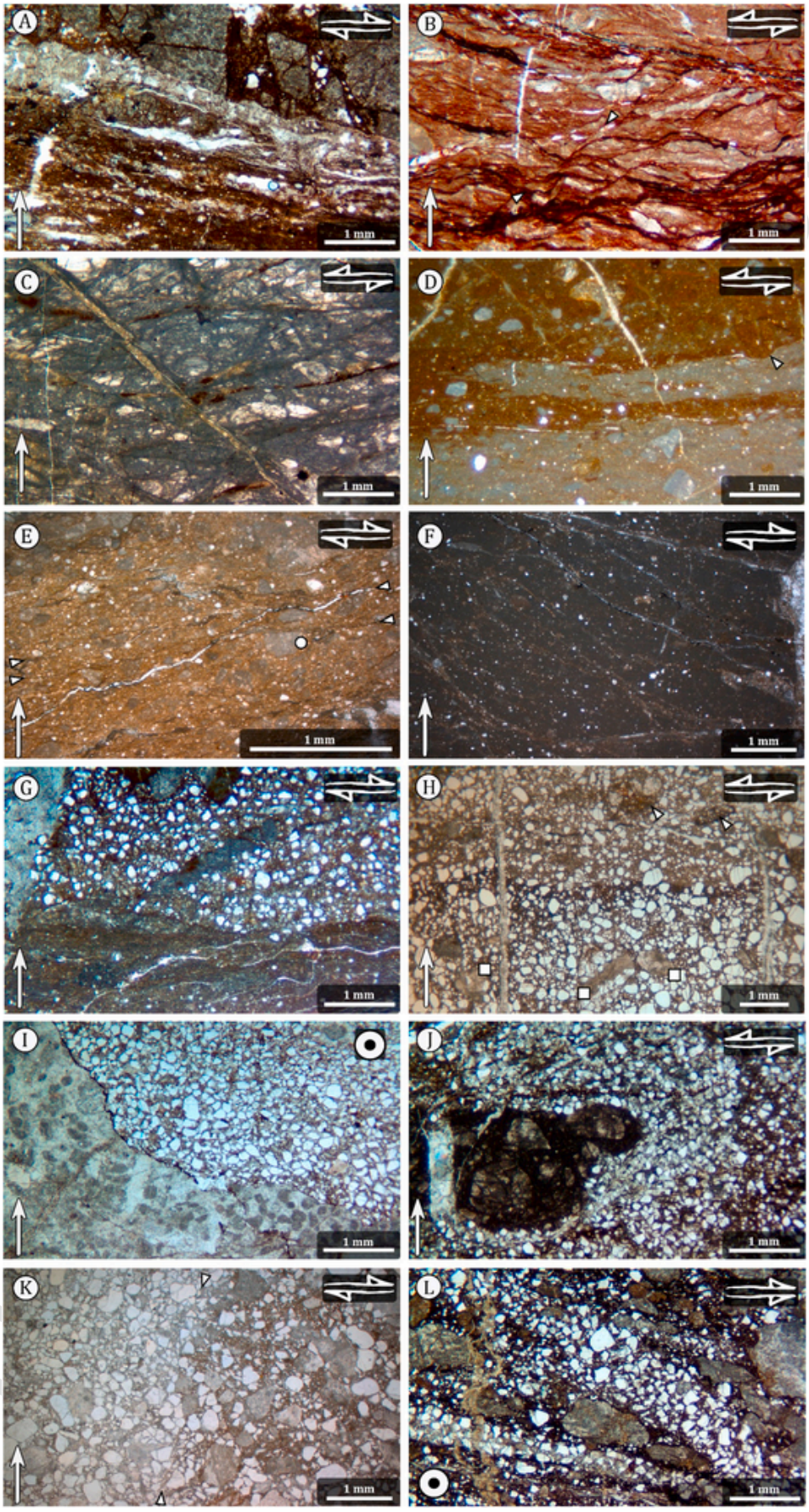
A
B
C
D
E
F
G
H
I
J
K
L
1 mm

Fig. 5.

Optical photomicrographs of the fault rocks located in the ENSZ. Arrows in lower left indicate the top of the succession, shear sense is indicated in upper right. Locations are indicated in Fig. 10C and 11. (A) Huergas-derived quartz cataclasite (dark, below) in contact with Láncara-derived cataclasites (dark, above), separated by a calcite vein. Note the presence of scarce quartz grains within the Láncara cataclasites. White circle is a resin bubble. Location W of Vozmediano. (B) Alba Fm. wackestone with crosscutting calcite veins and dissolution seams. Note Riedel-like surfaces (R_1) consistent with nappe transport sense (white triangles). Location W of Valdoré. (C) Portilla-derived cataclasite with locally twinned fragments. Location SE of Corniero. (D) LQz-U with a well-defined colour banding and cataclasite fragments. Note that the upper boundary of the dark band has been modified by dissolution (triangle). Location SW of Velilla. (E) LQz-U limestone fragments (white circle) truncated by surfaces (white triangles) that have undergone frictional sliding and dissolution. Location W of Velilla. (F) Compact LQz-U with homogenised carbonate matrix and fragments, rendering them virtually unrecognisable in optical microscopy. Location W of Velilla. (G) Detail of the sharp contact between the LQz-U (dark, below), and the QzLD-B (light, above). Note the absence of a strain gradient between both tectonites. Location W of Velilla. (H) QzLD-B with a matrix formed by calcite-cemented rounded and fractured quartz grains and limestone fragments of diverse origin. Most notably, an echinodermal quartz-bearing limestone derived from the Ermita Fm. (white squares), and limestone cataclasites derived from the Láncara Fm. (white triangles). Location NW of Velilla. (I) Detail of the contact between Láncara Fm. and a quartz sand-rich dyke cemented by calcite, found 2 m above the thrust surface. Note the corroded boundary of the limestone, suggestive of a chemically aggressive fluid during injection. Location N of Verdiago. (J) Santa Lucía Fm.-derived veined cataclasite fragment with a corroded boundary present in the QzLD-B. Location E of Argovejo. (K) Subvertical quartz-rich dyke crosscutting QzLD-B, richer in limestone fragments, with crackled cement. White triangles mark the subtle dyke-breccia contact. Location N of Velilla. (L) Bifurcating quartz sand-rich dykes crosscutting earlier quartz-bearing cataclasites. Location NW of Sabero. (For interpretation of the references to colour in this figure legend, the reader is referred to the Web version of this article.)

calcite matrix with variable quartz content (Fig. 5C). Limestone fragments are usually twinned, and display their longest dimension subparallel to bedding (Arboleya, 1999).

Present only locally, deformed mudstones of the Alba Fm. in the footwall display abundant subhorizontal and subvertical calcite veins, and subhorizontal continuous and anastomosing dissolution seams that define a penetrative tectonic planar fabric. Local development of oblique shear fractures is consistent with the tectonic transport (Figs. 2 and 5B, Riedel shear fractures (R_1); Rutter et al., 1986). Dissolution seams and R_1 surfaces are enriched in iron oxides relative to the matrix. Mutual crosscutting relations attest to a cyclic process of dissolution, vein opening and calcite precipitation.

Overlying the previous fault rocks there are limestone ultracataclasites with quartz fragments (LQz-U) which form a continuous 20–40 cm-thick layer. Carbonate fragments display smooth and rounded margins, and are formed by a homogeneous dark fine-grained micrite with euhedral authigenic quartz crystals and local evidence of partial or total silicification (see Supplementary Figure 2). Other fragments preserve previous cataclasites (Fig. 5D, Supplementary Figure 2), deformed echinoid ossicles and glauconite (see Supplementary Figure 2). Fragments are petrographically similar to the Ermita-derived protocataclasites and to the Láncara-derived cataclasites, but an unambiguous identification of their parent source is not possible. Some of the carbonate fragments display a mantled structure with elongated tails of smaller fragments (Fig. 6B&C; *cf.* Smeraglia et al., 2017). Quartz fragments are angular and usually monocrystalline. Fragments are embedded in an extremely fine-grained matrix (< 3 μm) dominated by calcite, quartz and minor and variable amounts of clay, apatite, Fe–Ti oxides and zircon (Fig. 6C&D, Table 2). In some samples, the matrix has been partially silicified.

LQz-U are often characterised by a planar fabric, a feature already recognized by Arboleya (1989), which results from a variety of factors not always concomitant (Fig. 4B). Firstly, the presence of dissolution seams enriched in small quartz fragments, clay minerals and Fe–Ti oxides. These surfaces form a flattened anastomosing pattern that wraps larger limestone and cataclasite fragments (Fig. 6B&C). Secondly, shear localization within the ultracataclasites, which results in thin layers where the porosity increases, filled by randomly oriented phyllosilicates (Table 2, Fig. 6D). This results in variations in the Ca–Si–Al–K–Fe content, a compositional banding already recognized by Arboleya et al. (1999) (Figs. 5D and 6B). The mineralogy of such bands is similar to that of dissolution seams. The bands are usually thick (500μm–3 mm), and have variable lateral continuity (cm–m). Their abrupt lateral termination resembles microfolds on visual inspection, but no evidence of folding is found at the microscale (Fig. 5D). They crosscut earlier veins, evidencing a process of reworking by cataclasis within the previously formed ultracataclasites, further supported by the presence of fragments of earlier cataclasites (see Supplementary Figure 2; Arboleya, 1989). The undulating boundaries of these bands suggest that LQz-U behaved plastically to a certain extent during at least part of the subsequent deformation. A third contributing factor to the fabric in the rock is the local development of thin calcite veins forming a low angle with the thrust surface (Arboleya et al., 1999). In some localities the planar fabric is absent and the ultracataclasites are formed by a homogeneous mixture of the aforementioned fragments and matrix (Fig. 5F). FSCP of the limestone fragments present in the most comminuted areas display a power law distribution of $\varnothing_{eq}$ with a D_{3D} in the order of 3.30–3.56 (Table 1 and Fig. 7B). FSCP of the quartz fragments display a D_{3D} in the order of 3.02–3.38 (Table 1 and Fig. 7C).

In the hangingwall, quartz-rich limestone and dolostone breccias (QzLD-B) constitute a tabular continuous interval with 1–4 m lateral thickness fluctuations (Fig. 4D). Their location is variable, but their contacts are always neat (Figs. 4C and 5G). Most usually, they appear on top of LQz-U, but in other areas they are found within them, within the Alba Fm., or on top of LD-BC (see Supplementary Figure 3). They are formed by angular limestone and dolostone fragments displaying sedimentary facies of the Láncara Fm., but also bioclastic and sandy grainstones, individual fossils and quartzarenites likely derived from the underlying Ermita and Nocedo fms. in the footwall (see Supplementary Figure 2). Fragments of LD-BC and LQz-U are also present (Fig. 5H, Supplementary Figure 2). Láncara-derived fragments are varied at the outcrop and thin section scale, despite the homogeneity of facies in the overlying undeformed host-rock, which suggests a process of intense mixing. Most fragments lack intragranular fractures. Fragment boundaries are often irregular, with evidence of corrosion due to the presence of chemically active pore fluid (Fig. 6F).

The matrix of the rock is formed by well-sorted rounded and sub-rounded detrital quartz grains (Figs. 5H and 6E). Quartz grain boundaries are often slightly corroded, a feature well known from sandstones with carbonate cement (Burley and Kantorowicz, 1986). The original quartz grains are locally crushed into smaller and more angular fragments. In unfractured areas quartz grains are cemented by calcite and rarely in contact with each other, though locally displaying intragranular extension fractures (Fig. 6E). In areas with incipient cataclasis, cement is crackled and the resulting porosity partially filled with clay minerals and Fe–Ti-oxides (Fig. 6F; Table 2). In fractured areas, both the cement and quartz grains have undergone an intense process of comminution reaching grain sizes < 3 μm. Many of the larger quartz fragments preserve a partial rim of the earlier calcite cement (Arboleya, 1999). FSCP of the quartz grains follows a log-normal distribution of $\varnothing_{eq}$ (Fig. 7D). In fractured areas the distribution has been partially modified into a power law distribution with a D_{3D} in the order of 2.48–2.73 (Table 2 and Fig. 7D). FSCP of the carbonate fragments dis-

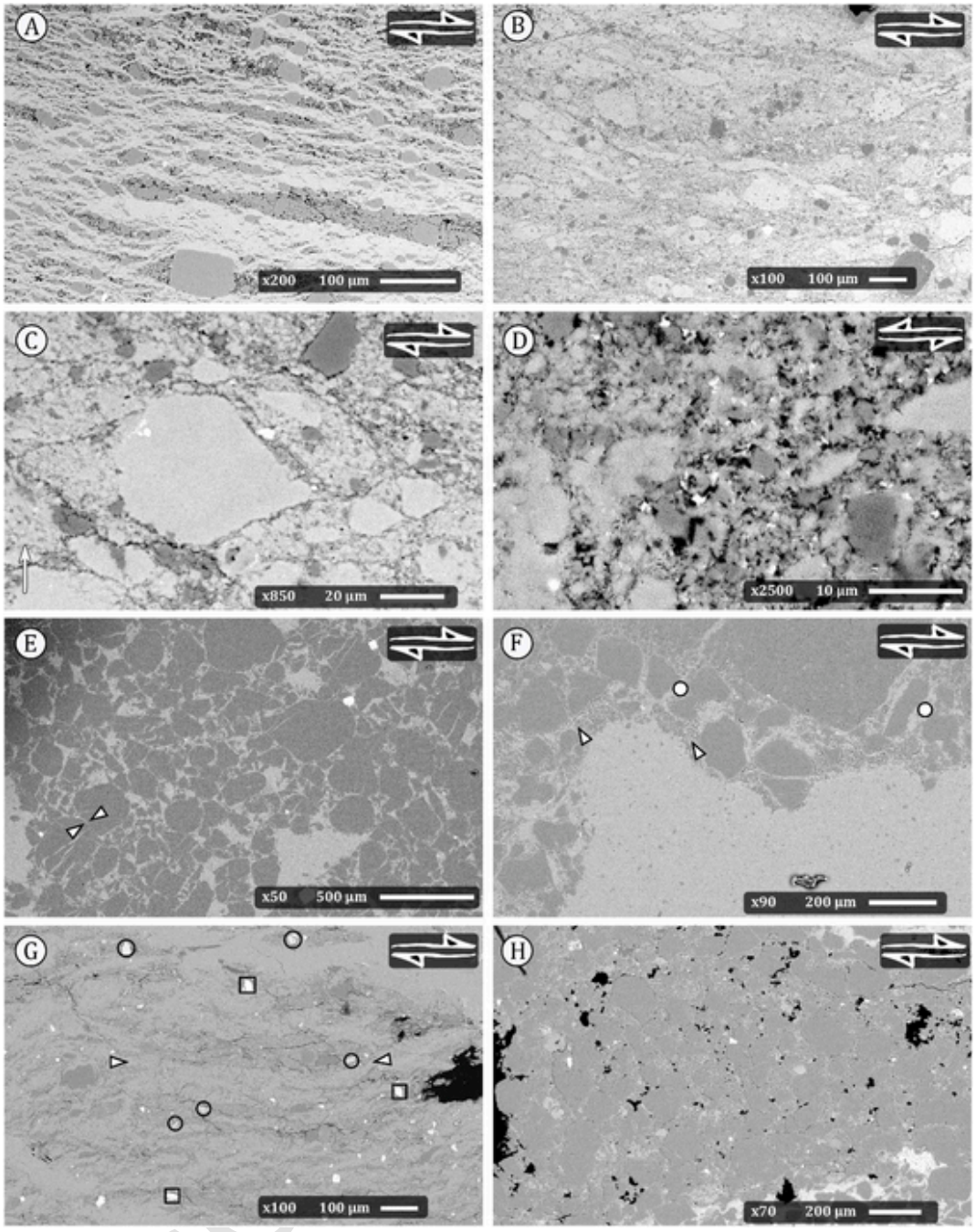

Fig. 6. Backscattered electron photomicrographs (BSE) of the fault rocks located in the ENSZ. The top of the succession is at the top in all photos: shear sense is indicated in upper right. Locations are indicated in Fig. 10C and 11. (A) Huergas-derived quartz cataclasite (dark) with a planar fabric caused by thin subhorizontal calcite veins (light). Location W of Voz-mediano. (B) LQz-U with a penetrative planar fabric defined by darker ultracataclasite intervals and anastomosing dissolution seams. Note the presence of authigenic quartz crystals in some of the fragments. Location SW of Velilla. (C) Detail of a limestone fragment in LQz-U with anastomosing dissolution seams. Dark and thin ultracataclasite intervals display clay-filled porosity. Location SW of Velilla. (D) Fine-grained ultracataclasite matrix formed by calcite (light) and quartz (dark), with minor Fe–Ti-oxides and clay-filled porosity. Note the calcite attached to quartz grains, suggesting they are derived from authigenic crystals. Location NW of Sabero. (E) Rounded quartz grains forming the matrix of the QzLD-B. Note the cement between grains and filling intragranular fractures, the absence of simple shear deformation and the indentation of some of the quartz grains (white triangles). Location N of Velilla. (F) Carbonate fragments in QzLD-B. Note the corroded boundary of the limestone fragment (light, below), as opposed to the dolostone fragment (dark, above), and the calcite rim preserved by some of the quartz grains in the matrix (white circles). Porosity-filling clay minerals within cracks in the matrix (white triangles). Location N of Crémenes. (G) Prioro-derived quartz ultracataclasite with small Fe-oxide (framed) and apatite fragments (encircled) embedded in a clay-rich matrix. Note the planar fabric defined by subhorizontal interconnected calcite-rich veins with irregular boundaries (white triangles). Location N of Ferreras. (H) Partially crushed quartz grains in a quartz-rich sill at the base of the Santa Lucía Fm. The matrix between large grains is formed by crushed quartz, calcite cement and clay minerals. Note the clay matrix (bright) in the lower and upper right. Location NE of Argovejo.

play a power law distribution with a D_{3D} of 3.06 (Table 1 and Fig. 7D).

In certain areas of the hangingwall, quartz sand-rich (up to 60% mode) lithosomes form an interconnected network of variably-oriented dykes and sills injected into the ENSZ (Figs. 4F and 8, see Supplementary Figure 3). Bedding-parallel tabular sills are often continuous at the scale of several tens of meters, and are usually restricted to thicknesses <50 cm (Fig. 8A and Supplementary Figure 3). In contrast, dykes oblique or normal to bedding display both tabular and irregular morphologies, and can reach structural heights of up to 20 m over the

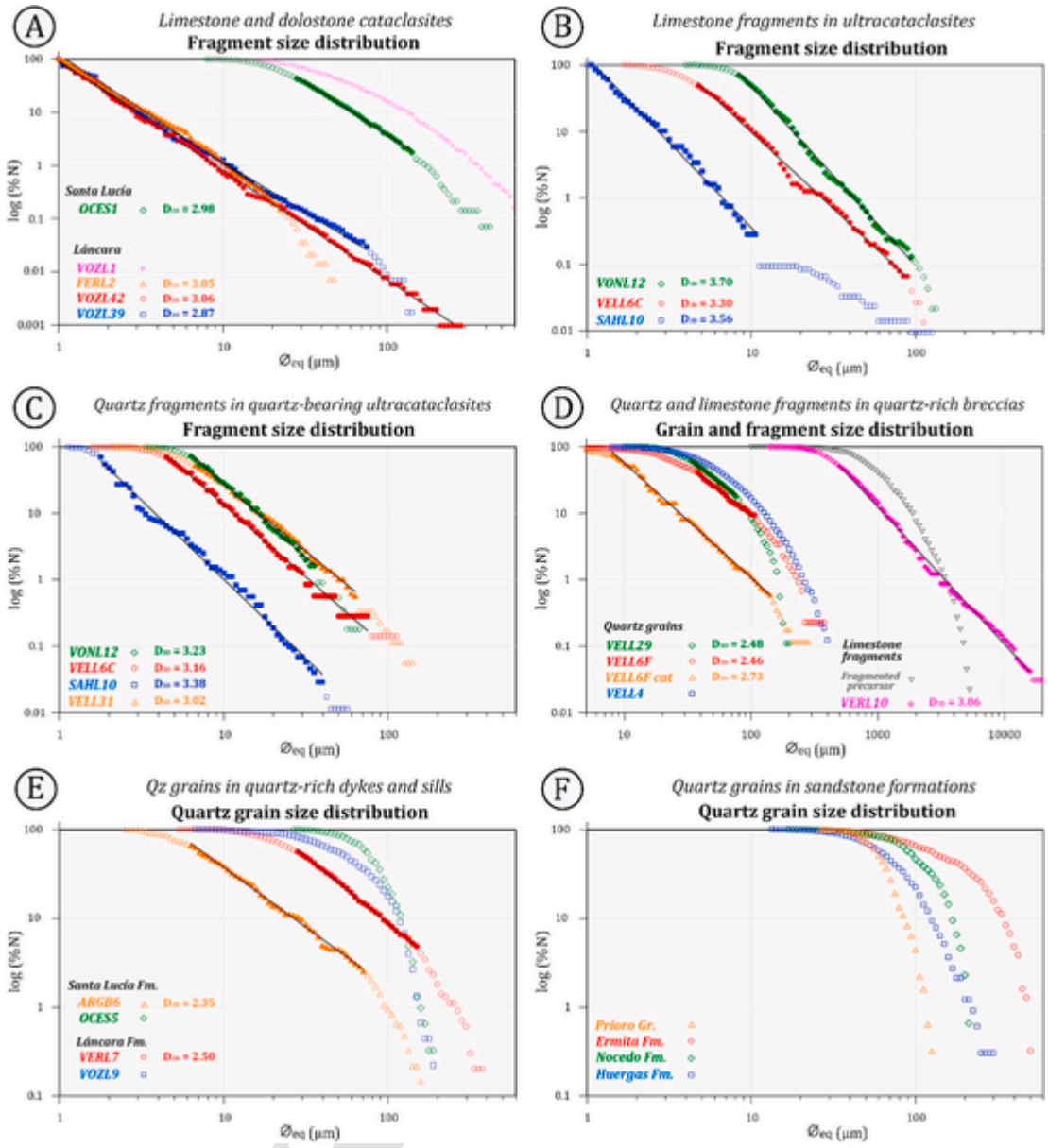

Fig. 7. Quartz grain and carbonate fragment size distributions and histograms. In samples where a partial power law distribution is observed, the size range that conforms to it is highlighted by closed symbols. D_{3D} denotes the three-dimensional fractal dimension of the distribution.

Table 2
Average compositions (%) of the clay matrix found in the LQz-U and QzLD-B as determined from EDX measurements. Contamination with fine-grained quartz, calcite and Fe–Ti-oxides is inevitable, so the Si–Ca–Fe–Ti should be regarded with care. K enrichment suggests that the clay fraction is formed by illite and/or smectite.

Rock	Na_2O	MgO	Al_2O_3	SiO_2	P_2O_3	K_2O	CaO	Mn_2O_3	TiO_2	FeO
LQz-U	0.0	0.9	21.6	34.5	0.0	8.9	27.2	0.0	0.0	6.9
QzLD-B	0.2	1.7	21.4	38.5	0.8	7.0	13.0	0.4	2.0	15.0

ENSZ (Fig. 8A). Large dykes often display at their margins secondary quartz-filled fractures without shear displacement which generate a characteristic jigsaw texture (Figs. 4G and 7D). In some areas, a dense framework of thin quartz sand-filled fractures crosscut the host Láncara Fm. in the absence of a well-defined nearby dyke, resembling a crackle breccia without shear strain. Locally, new dykes have crosscut earlier dykes and QzLD-B (Figs. 4D, 5I and 6F; see Supplementary Figure 3). FSCP of the quartz grains approximates a log-normal distribution, except in fractured volumes which display a D_{3D} in the order of 2.50 (Table 1 and Fig. 7E).

5.3. Fault rocks located between Argovejo and Ferreras (front of the Esla Nappe)

In this area the base of the nappe is formed mostly by Devonian limestones (Santa Lucía and Portilla formations). Láncara Fm. also

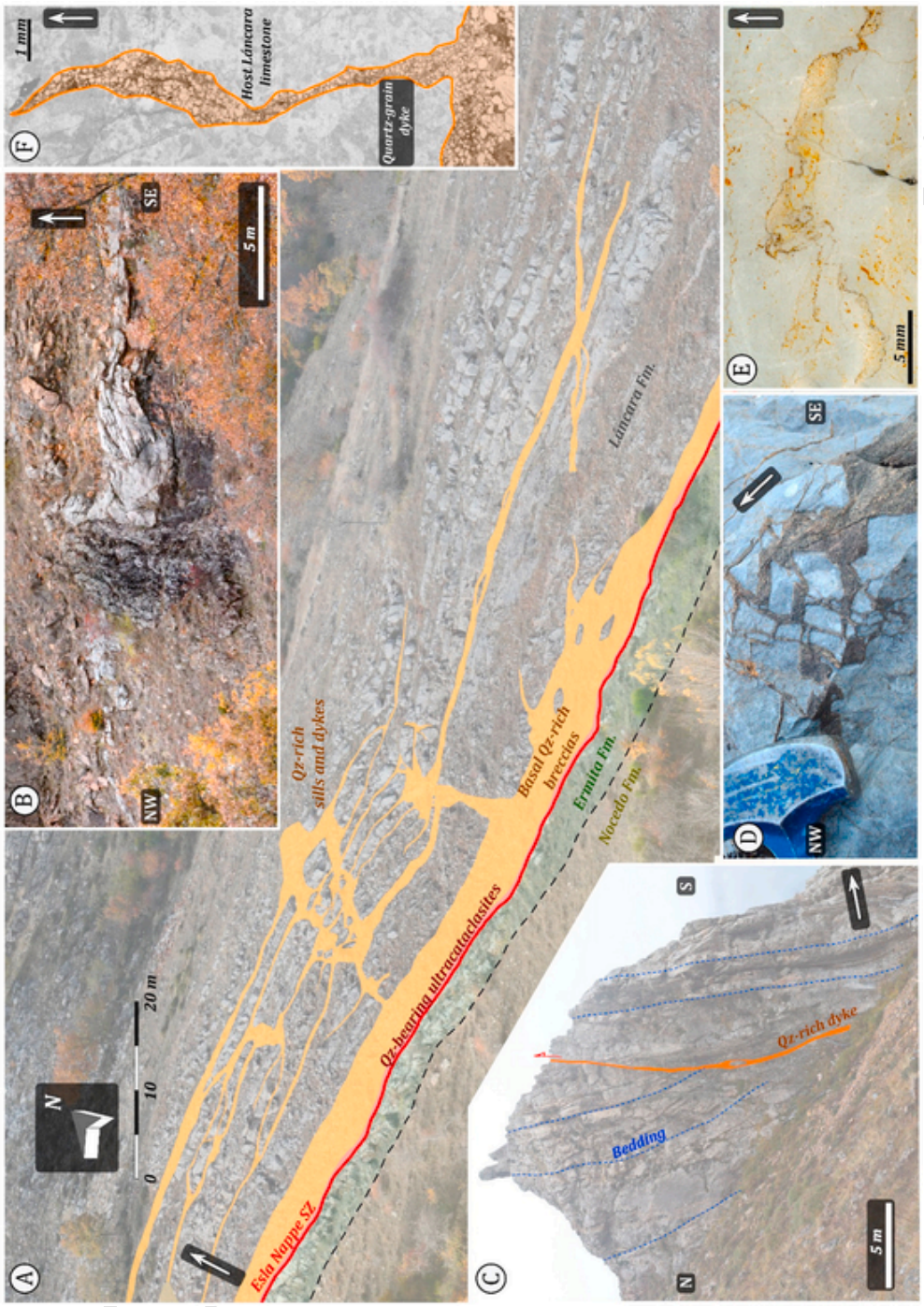

Fig. 8. Field (A–D) and microscope (E–F) photographs of characteristic features of the quartz sand-rich injections in the ENSZ. Transport sense in the ENSZ is roughly normal to the picture plane (A–D) or to the left (E–F). Arrows indicate the top of the succession. Locations are indicated in Fig. 11 (A) Slope north of Valdoré with excellent outcrops of the basal quartz sand-rich breccias and the overlying network of dykes and sills, which in this location penetrate 20 m into the hangingwall. (B) Slope East of Valdoré displaying a 4 m-thick quartz sand dyke (dark-coloured) sourced from the Nocedo Fm., cutting across the Ermita Fm. (light limestones) and feeding the quartz-rich fault rock assemblages injected into the Esla Nappe. (C) 20 cm-thick quartz sand dyke injected along a small-scale thrust surface rooted in the ENSZ, located some 20 m below. Location E of Vozmediano. (D) Jigsaw texture in a hydraulic breccia with injected quartz sand matrix, located in the boundary of a larger dyke. Location E of Velilla. (E) Quartz sand-rich injected along a previously formed stylolite. Sample was collected 8 m above the ENSZ. Location N of Verdiago. (F) Small-scale injection of quartz sand grains into the limestones of the Láncara Fm. in the hangingwall. Location SW of Velilla.

crops out in the South-easternmost sector. The footwall is invariably formed by shales, sandstones and limestones of the Prioro Group (Figs. 1B and 3).

In the contact between the Láncara Fm. and the Prioro Gr., the footwall is formed by quartz-bearing ultracataclasites. They form a 2–5 mm-thick layer made of angular quartz, Fe-oxide and apatite fragments embedded in a clay-rich matrix crosscut by thin (<100 μm) extension calcite veins subparallel to the thrust surface, interconnected through vertical hydrofractures (Fig. 6G). Their precipitation has accomplished over 40% local vertical dilation, and their irregular boundaries (Fig. 6G), the presence of small ultracataclasite flakes within them, and the blunting of veins opened in the hangingwall, attest to the bulk ductile behaviour of the ultracataclasites.

The base of the Láncara Fm. in the hangingwall is formed by carbonate breccias and cataclasites similar to the ones observed West of Vozmediano (Section 5.1). Their FSCD displays a power law distribution with a D_{3D} of 3.05 (Table 1 and Fig. 7A). Cataclasites are also found at the base of the Santa Lucía Fm., with a very similar FSCD (D_{3D} = 2.98, Table 1 and Fig. 7A).

Quartz-rich limestone breccias form a 10–20 cm-thick layer at the base of Santa Lucía-derived cataclasites. They are petrographically similar to the QzLD-B of the Láncara Fm., but formed by more scarce (ca. 20%) angular and sub-rounded limestone fragments derived from the Santa Lucía Fm., either pristine or in the form of cataclasites, and with a smaller quartz grain size (Figs. 5J–6H). The transition from the quartz-rich breccia facies towards the limestone cataclasites above is gradual at the microscale. The fragments closer to the limestone cataclasites are just barely detached from each other, and can easily be refit together. FSCP of the quartz grains approximates a log-normal distribution, but in fractured volumes this distribution has been modified into a partial power law distribution with a D_{3D} in the order of 2.35 (Table 1 and Fig. 7E).

Quartz-rich sills and dykes display similar characteristics to those hosted by the Láncara Fm., and also reach several tens of meters into the hangingwall (Fig. 4H and Supplementary Figure 3).

6. Orientation of the dykes and relation with other tectonic structures

The orientation and location of the quartz sand-rich injections found in the Láncara and Santa Lucía formations indicates that many of them follow pre-existing planar discontinuities in the hangingwall. These discontinuities were opened and injected with a mixture of host fragments floating in quartz sand grains. Among these surfaces are bedding planes, decametric thrust surfaces rooted in the basal shear zone of the nappe (Fig. 8C), as well as joints and minor high-angle faults. At a smaller scale, injections also intruded the host rock following stylolites (Fig. 8E).

Oblique injections display diverse orientations with respect to the estimated transport sense (N 30° E in present-day coordinates; Fig. 2). When the nappe rests on a portion of the footwall where the Nocedo Fm. is present, always at a maximum distance to the contact of 10 m, transport-parallel and -oblique sets dominate, with a large proportion (*ca.* 70% of total) of high-angle dykes (*i.e.* >60° with respect to bedding; Fig. 9A). When the nappe rests on top of the Ermita or Alba formations without the presence of the Nocedo Fm. below, transport-normal and -oblique sets dominate, with a lower proportion of high-angle dykes (55% of total; Fig. 9B). Finally, when the nappe rests on top of

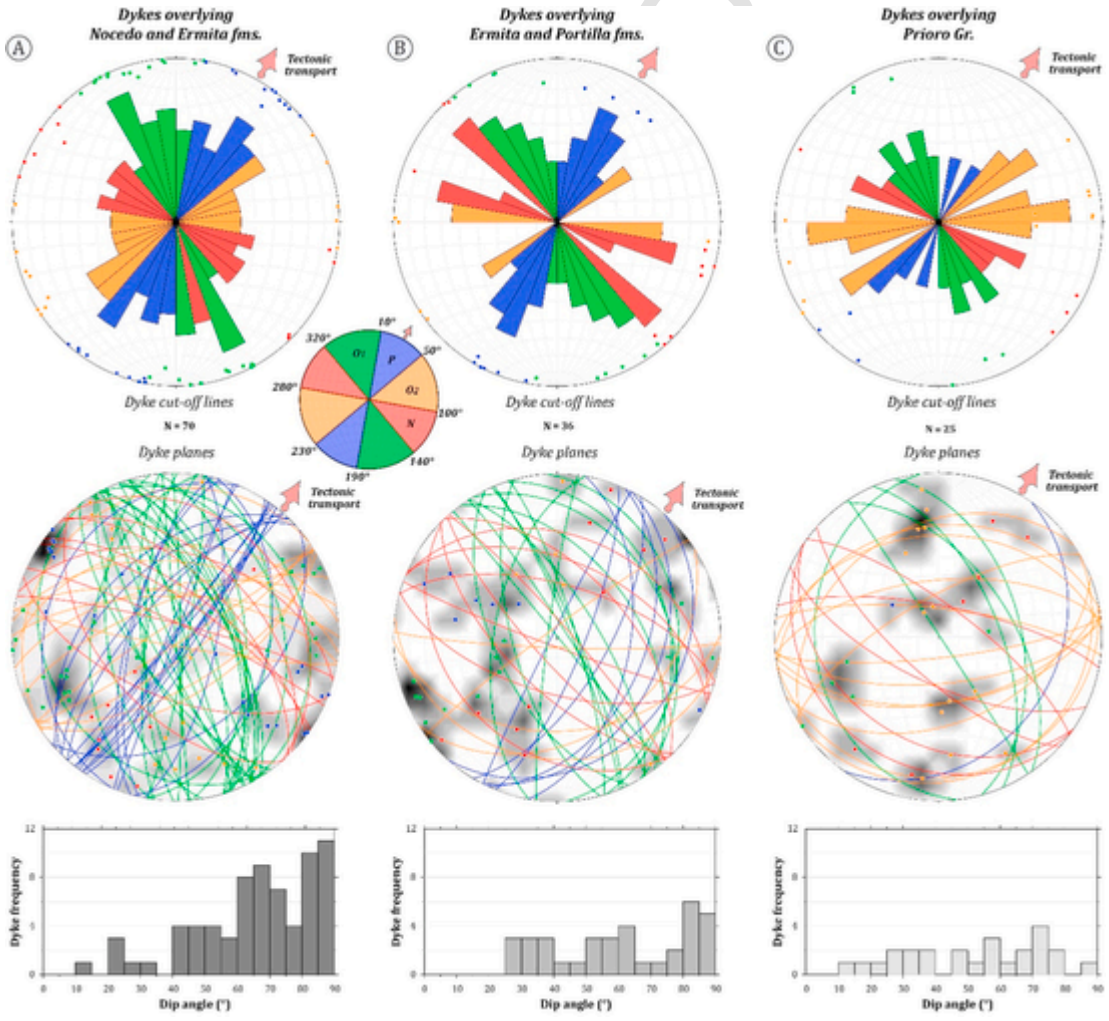

Fig. 9. (A–C) Lower-hemisphere equal-area stereoplots displaying the restored orientations of the dyke cut-off lines with bedding (1st row), dyke planes (2nd row) and dyke dip frequency plots (3rd row), for areas underlain by the Nocedo and Ermita fms. (A), Ermita and Portilla fms. (B) and Prioro Gr. (C). Note that rose diagrams are constructed so that the number of data is proportional to the area of the wedges, not to their length. The small coloured stereoplot illustrates the division of dykes in sets with transport-parallel (P, blue), transport-normal (N, red) and transport-oblique (O1–O2, green-orange) dykes. (For interpretation of the references to colour in this figure legend, the reader is referred to the Web version of this article.)

the Prioro Group, the transport-oblique set dominates, with the lowest proportion of high-angle dykes (40%; Fig. 9C). There is no clear relation between dyke strike and dip angle in any of the areas.

7. Discussion

7.1. Deformation related to the emplacement of the Esla Nappe

The fault rock assemblages found in the ENSZ allow to constrain deformation processes and fluid conditions operating during the emplacement of the Esla Nappe. Deformation processes were different among lithologies in the hangingwall and the footwall, likely as a result of their different composition, rheology and fluid pressure conditions.

The Láncara Fm. in the hangingwall experienced the largest accumulated displacement-related strain, accommodated as distributed cataclastic flow in a <50 cm-thick band characterised by the presence of cataclasites with an extremely fine-grained matrix (down to 500 nm) formed through the disaggregation and grinding of the microcrystalline texture of the carbonate protolith (Fig. 5A). In the hangingwall Santa Lucía Fm., deformation also evolved through distributed cataclasis in a narrow zone located at its base. D_{3D} around 3.0 in the cataclasites is not consistent with the constrained comminution model of Sammis et al. (1987), and can in turn be explained by larger shear strains induced by shear localization (Table 1 and Fig. 7A; Sammis and King, 2007). $D_{3D} > 3.0$, as recorded in the ultracataclasite intervals, cannot be described as fractal or self-similar (Heilbronner and Keulen, 2006), and are likely the result of scale-dependant comminution processes, such as large particle abrasion or selective breakage (VONL12 in Table 1 and Fig. 7B; Blenkinsop, 1991; Storti et al., 2003).

In contrast, competent limestones of the Ermita and Portilla fms. in the footwall were deformed through different deformation processes. Incipient cataclasis affected an interval of 60–100 cm where coarse calcite crystals are locally twinned, a feature studied by previous authors. Arboleya et al. (1999) attributed the twinned cataclastic grains to an incipient ductile deformation following ultracataclasite development. In contrast, Rowe and Rutter (1990) focussed on the twins present in the uppermost Portilla Fm. in contact with the ENSZ, and attributed them to an earlier phase of layer-parallel compression that preceded strain localization at the ENSZ. Observations by Rowe and Rutter (1990) and the calcite twinning locally observed in coarse-grained veins hosted by the fault rocks suggest that twinning was also an operative process during the subsequent emplacement of the underlying Corniero Nappe. Therefore, it is likely that twinning activity took place prior, during and subsequently to the emplacement of the Esla Nappe. Demurtas et al. (2019) have shown that in calcite and dolomite gouges experimentally deformed at low confining pressures (17.5 MPa), twins can develop in conjunction with brittle fracturing during cataclastic flow. However, twining requires high stresses to operate (*e.g.* Rutter, 1995) and although its occurrence in the cataclasites evidences high stress concentrations at fragment contacts, it may not be regarded as the mechanism favouring the maintenance of strain localization during nappe movement.

Sandstone beds within the Huergas Fm. in the footwall localised cataclastic flow in a layer with a thickness $\ll$10 cm directly below the thrust contact (Fig. 10A). Sandstone layers within the Prioro Gr. have developed an ultracataclasite with a large content of clay minerals in the matrix, which is barely 5 mm-thick. On the other hand, the Alba Fm. was mostly deformed through a cyclic interplay of pressure solution and hydrofracturing associated with calcite vein precipitation.

The most complex deformation is recorded in the 20–40 cm -thick intervening quartz-bearing carbonate ultracataclasites (LQz-U) located at the thrust contact (Fig. 10B and C). There, fragments of the protocataclasites and quartz grains of the Ermita Fm., and possibly fragments derived from the Láncara Fm., were incorporated into a more mature cataclastic flow, and grinded down to form ultracataclasites where several cycles of cataclasis are identified (Fig. 5D–F and 6B-D; see Supplementary Figure 2). Their large D_{3D} (Fig. 7B&C) in excess of 3.0 suggest the activation of scale-dependant (non-fractal) selective comminution processes following intense shear localization (Blenkinsop, 1991; Storti et al., 2003; Sammis and King, 2007). Planar and anastomosing dissolution seams formed by a mixture of quartz, calcite and clay minerals, responsible of the planar fabric of the ultracataclasites, attest to the importance of episodic dissolution creep in the deformation history (Figs. 5D and 6B&C; Tesei et al., 2013; 2014; Smeraglia et al., 2017). In some cases, a complex interplay between dissolution and frictional sliding on the same surfaces is recorded in the ultracataclasites (Fig. 5E). The presence of thrust-parallel dissolution seams within thrust-related fault rocks has been previously explained by at least two mechanisms. The first one, proposed by Kennedy and Logan (1997), considers that the formation of dissolution seams is influenced by pre-existing anisotropies more than by ambient stresses. The second one considers that the fault rocks at the thrust contact are subjected to layer-normal compression due to their weak rheology, either compositionally-related or influenced by high pore fluid pressures (Byrne and Fisher, 1990; Fagereng, 2013). In the case of the LQz-U of the ENSZ, there are no obvious pre-existing anisotropies within the fault rocks, and so we regard the thrust-parallel dissolution seams as the result of periods of increased fluid pressure. In summary, an interplay of cataclasis, dissolution, and localised frictional sliding is observed in this fault rock assemblage with an overall ductile behaviour of the matrix. Variations in the deformation mechanism likely resulted from secular variations in the ultracataclasite pore fluid content and pressure: strain accumulation accommodated by ongoing frictional wear and cataclasis was transiently assisted by superimposed dissolution creep during periods of increased pore fluid content (*e.g.* Wojtal and Mitra, 1986; 1988; Tesei et al., 2013).

Microstructural observations are consistent with late transient high pore fluid pressures that caused a local vertical dilation of the weak Huergas and Prioro cataclasites and Alba deformed wackestones in the footwall, as well as the transitional LQz-U, through hydrofracturing followed by calcite precipitation and sealing (Figs. 5A and 6A&G). In some cases, the released fluids also entrained quartz grains from the footwall, which were subsequently comminuted within the ultracataclasite layer, as proposed by Arboleya (1989). Progressive fluid pressure increase eventually overcame the minimum principal stress and the tensile strength of the ultracataclasites, leading to hydrofracturing and vein precipitation (*e.g.* fault-valve mechanism, Sibson, 1990). Nonetheless, we consider that the fluid pressure increase and hydrofracturing need not have been related necessarily with the seismic cycle, but could be the result of a foreland-directed pulsating fluid migration associated to tectonic loading (Winslow, 1983; Palladino et al., 2016), clay mineral dehydration in the footwall, or pore closure associated with pressure solution and cementation (Helset et al., 2002).

Fluid-rock interaction during deformation is further exemplified through mineral precipitation and replacement, such as iron oxides precipitated along dissolution seams and R_1 surfaces in the Alba Fm (Fig. 5B). or as micrometre-sized crystals in the ultracataclasites of the Prioro Gr. (Fig. 6G). The texture and location of randomly oriented clay minerals filling open porosity in the LQz-U and QzLD-B suggest that they were precipitated from Si-rich fluids (Table 2, Fig. 6D). The carbonate fragments of the ultracataclasites display abundant authigenic quartz crystals, a feature that is not observed in any other fault rock assemblage and likely related to thrust-parallel fluid infiltration by Si-rich fluids or to the dissolution of quartz and clay minerals present within the ultracataclasites (Fig. 6B and Supplementary Figure 2; Molenaar and de Jong, 1987).

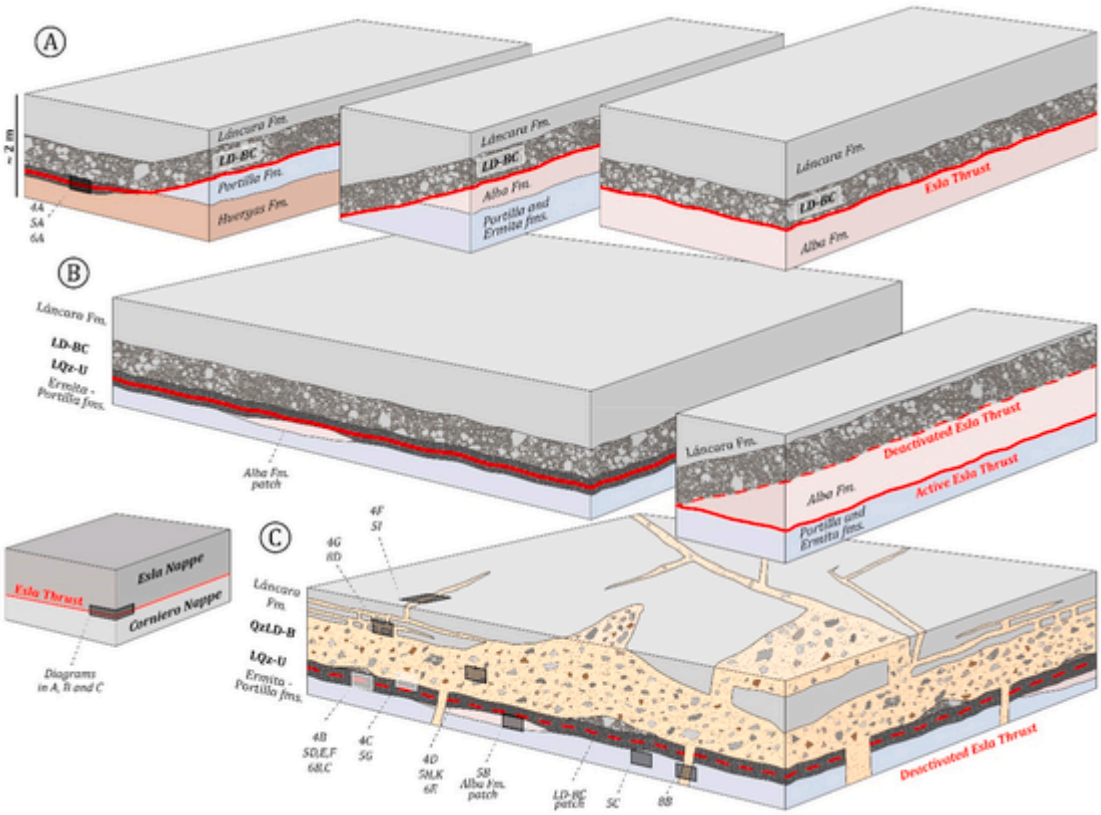

Fig. 10. Idealised diagram depicting the evolution of the fault rock assemblages of the ENSZ. Transport sense towards the right. Note that the diagram scale is approximated. The context of several photographs of Figs. 4–6 and 8 is indicated in (C). (A) Original position of the Esla Nappe over the Huergas Fm. (at the rear) and the Alba Fm. (at the front). The uppermost structural position of the nappe (resting on the Bashkirian Prioro Gr.) is not shown in the figure. The Láncara Fm. of the hangingwall develops at its base the LD-BC, and the Huergas Fm. of the footwall develops quartz-ultracataclasites in the contact. (B) Once the footwall ramp is broken, with a new detachment at the base of the Alba Fm., the Láncara Fm. of the hangingwall is emplaced over the Ermita Fm. (where present) and the Portilla Fm. of the footwall. Note the patches of Alba Fm. left behind (not to scale). The LQz-U are developed in the ENSZ as a result of nappe emplacement. (C) Once the footwall ramp is again broken, with a new detachment at the base of the Portilla Fm. (not shown, see text for explanation), a series of quartz-bearing injections sourced from the footwall intrude the deactivated ENSZ, leading to intrusion brecciation of the base of the hangingwall (QzLD-B) and the development of a system of interconnected clastic dykes and sills. Note the preserved patches of LD-BC, otherwise fragmented and incorporated into the QzLD-B. A similar process is envisioned for the more frontal area where the Santa Lucía Fm. is located at the base of the hangingwall (not shown in the figure).

7.2. Origin of the quartz sand in the quartz-bearing ultracataclasites, breccias and dykes

Quartz grains present in the LQz-U are derived from at least three sources: (i) the quartz-bearing grainstones of the uppermost Ermita Fm. in contact with the Esla Nappe, (ii) the authigenic quartz crystals present in most of the limestone fragments, and (iii) small-scale quartz injections derived from the footwall. During the emplacement of the Esla Nappe over the footwall flat developed on top of the Upper Devonian formations, located between Vozmediano and Argovejo, cyclic small-volume injections of quartz grains derived from the footwall intruded the deforming cataclasites and ultracataclasites at the base of the nappe (Q-veins of Arboleya et al., 1999). Quartz grains were subsequently disaggregated and incorporated into the cataclastic flow, before being subsequently injected by new Q-veins (Fig. 5L; Arboleya, 1989; Arboleya et al., 1999). The lower quartz content and variability of limestone fragment facies in the ultracataclasites (LQz-U), in comparison with the quartz-rich breccias (QzLD-B), preclude the interpretation of the former as the deformed counterpart of the latter.

Quartz grains in quartz-bearing breccias and injections of the Esla Nappe have traditionally been considered an exotic phase injected from an underlying source (van der Meer Mohr, 1969; Arboleya, 1989), as both Láncara and Santa Lucía fms. of the hangingwall lack quartz grains, except as a very fine-grained minor phase (< 3%).

A series of evidence strongly suggest that the Upper Devonian Nocedo and Ermita formations acted as the source parent units from which the injected quartz sand in the Láncara Fm. was derived, in agreement with cathodoluminescence data of Arboleya et al. (1999). Firstly, detailed mapping indicates that the Láncara-hosted quartz-rich fault rock assemblages are exclusively developed in the areas where the nappe rests on top of the Upper Devonian sandstones of the Nocedo and Ermita formations, or at a maximum lateral distance of 500 m (Fig. 11). Secondly, FSCP of quartz sand grains in the Devonian formations, basal breccias, dykes and sills display a similar log-normal distribution with overlapping grain sizes (Table 1 and Fig. 7F). While this is not an unequivocal evidence, it is consistent with the proposed interpretation. Thirdly, quartz sand-filled hydrofractures locally occur within the Ermita Fm. Finally, the upper part of the Nocedo Fm. frequently crops out as a massive reddish interval with no trace of sedimentary structures, which are common at the base and in other regions, suggesting a process of liquefaction and destruction of the sedimentary fabric (Duranti and Hurst, 2004). Moreover, a thick dyke sourced from the Nocedo Fm. truncates the overlying Ermita Fm. and reaches the base of the Esla Nappe, where it fed the matrix of the basal breccias and dykes (Fig. 8B).

The lithification degree of Nocedo and Ermita fms. at the time of emplacement is difficult to ascertain, as the lithification process is controlled by a myriad of factors (*e.g.* Bjørlykke, 1988). Preservation of cross-lamination within 1 m of the thrust contact suggests that at least the grainstones of the Ermita Fm. were sufficiently lithified in order to

Fig. 11. Geological map with the spatial distribution of the occurrence of quartz sand-rich dykes and sills injected along the base of the Esla Nappe. Location of the photographs in Figs. 4–6 and 8 is also shown.

sustain shear strain imposed by the nappe advance. The sandstones of the Nocedo Fm., deposited 65 Myr prior to the Esla Nappe emplacement (Fig. 3), were however not completely lithified as evidenced by the injections sourced from them. Poor lithification was likely restricted to certain intervals or patches and not to the whole formation, as sandstone fragments, in addition to loose quartz grains, are present within the breccias.

Santa Lucía-hosted quartz rich fault rock assemblages are developed in areas where the Esla Nappe rests on the Bashkirian Prioro Gr. (Fig. 3). The close spatial association between Prioro Gr. sandstones and the injections strongly suggests that they acted as the parent units from which the quartz was sourced. FSCP of the quartz grains in the Prioro sandstones is comparable in grain size and distribution to that of the Santa Lucía-hosted dykes, which is consistent with this hypothesis (Table 1 and Fig. 7F). The degree of sandstone lithification at the time is difficult to determine from the deposits (Bjørlykke, 1988), but their close relation with the injections suggests that they were still unlithified.

7.3. Breaching of the ENSZ

During the late stages of emplacement of the Esla Nappe, a series of large-scale hydrofracturing events breached the ENSZ. Fast fluid flow entrained liquefied quartz sand grains from the footwall, fluidizing and injecting them into the hangingwall through intrusion fracturing (Fig. 10C). The process generated a brecciated regional-scale sill at the base of the nappe, driven by the regional achievement of fluid overpressure conditions in excess of lithostatic values, as has been proposed for similar regional-scale subhorizontal injections (*e.g.* Vigorito and Hurst, 2010). In the case of the Esla Nappe, the lithostatic pressure was effectively the minimum principal stress, as expected in a foreland thrust belt. Thus, considering a minimum overburden of 4300 m, the required minimum fluid pressure would be in the order of 110 MPa.

Large fluid overpressures also caused the dilation of previously formed anisotropies in the hangingwall with an unfavourable orientation, leading to the injection of quartz-rich dykes and sills (Fig. 10C). The pervasive development of secondary hydrofractures around the dykes (Figs. 4G and 8D) and the relative scatter in the dyke orientations are typical of high pore fluid overpressures (Fig. 9; Cosgrove, 1995; Jolly and Sanderson, 1997). Injected fluids had a corrosive effect in the limestone fragments and walls (Fig. 5I&J and 6F), likely as a result of the siliciclastic nature of the parent units and the resultant fluid under-saturation in carbonate ion content (Swennen et al., 2012). Conversely, the decrease in CO_2 partial pressure during decompression following intrusion fracturing could have been the cause for the switch from corrosion to carbonate precipitation of the cement (*e.g.* Swennen et al., 2012).

The breccias display a significant contrast in the FSCD of quartz grains and limestone fragments. Whereas the former usually show log-normal distribution or low D_{3D} values, the latter have a high D_{3D} in the order of 3.06 (Table 1 and Fig. 7D). However, it is clear that such high value is not related to shear localization within the breccias, as in the ultracataclasites, given the low content in fine-grained matrix and the scarcity of shear fractures within the intervening quartz grains (Fig. 5H, J, K and 6 E, H). The high D_{3D} is also not in agreement with estimates for fluid-assisted hydraulic brecciation, usually characterised by restricted fragment sizes and D_{3D} below 2.40 (Blenkinsop, 1991; Jébrak, 1997). High D_{3D} values in excess of 3.0 have been reported for rocks subjected to highly energetic confined explosions (Jébrak, 1997; Barnett et al., 2011). Nonetheless, it is well known that the value of D_{3D} is not solely influenced by the fragmentation process or by the energy input. Other factors, such as the initial size distribution of the fractured volume, or the number of fracturing events, also play an important role (Blenkinsop, 1991). Though not preserved in the Esla Nappe, the limestones and particularly the dolostones of the Láncara Fm. at the base of the underlying Corniero Nappe and other Cantabrian nappes are heavily jointed, with the resulting fragments displaying a power-law distribution (Fragmented precursor, Fig. 7D). Thus, any fragmentation process affecting such volume could exploit the fracture network to produce any sized fragments independently of the energy input. We thus favour an origin for the Esla Nappe breccias related to the intrusion brecciation of a pre-fractured host rock driven by the sudden injection of highly pressurised fluids and sand grains derived from the footwall.

Following their formation, the breccias have barely accumulated any deformation. In many samples the quartz grains remain largely undeformed, with their FSCP following a log-normal distribution (Table 1 and Fig. 7D&E). The scarcity of well-defined simple shear fractures (Table 1 and D_{3D} of 2.73, Fig. 7D) suggests that no significant simple shear strain followed their formation. This is supported by the usually low D_{3D} (Tables 1 and 2.35–2.48) of fractured volumes, more consistent with tensile or mode I fracturing (Table 1 and Fig. 7D&E; Blenkinsop, 1991). Locally, new well-cemented dykes cut across earlier breccias with crackled cement, evidencing a new cycle of injection and cement precipitation following incipient deformation (Fig. 5K). Their local wavy boundaries and textural similarity suggest that earlier injections were not completely lithified at the time of subsequent intrusive events.

7.4. Timing of injections

The timing of quartz-sand injection is key in adequately understanding the deformation processes that facilitated the movement of the Esla Nappe, particularly in its final stages of emplacement. Several lines of evidence indicate that the Esla Nappe completely overlain the Upper Devonian and Carboniferous formations when the injections occurred, and that most of the strain associated with the emplacement of the Esla Nappe was recorded by the previously formed fault rock assemblages such as cataclasites and ultracataclasites (LD-BC and LQz-U). Firstly, Láncara-derived cataclasites (LD-BC) are present almost exclusively where the quartz sand-rich breccias (QzLD-B) are absent. Where the latter are present, cataclasites are preserved as patches below the quartz sand-rich breccias, or more frequently, as fragments within the breccia (Figs. 5H and 10C; Supplementary Figure 2; Arboleya, 1989). This demonstrates that the cataclasites preceded injections, and thus constitute the hangingwall fault rock assemblage generated as a consequence of the Esla Nappe displacement up to that moment. In contrast, where the Láncara Fm. of the Esla Nappe rests on top of the Carboniferous Prioro Gr., quartz-rich fault rock assemblages are absent. In the case of quartz-rich breccias hosted by the Santa Lucía Fm., the limestones that constitute the fragments (cataclasite fragments, Fig. 5J) display larger strains than the Santa Lucía Fm. from which they are detached (mostly protocataclasites), evidencing that emplacement-related cataclasites preceded the brecciation process. Secondly, the contact between QzLD-B and either LQz-U or LD-BC is very sharp, without a strain gradient (Figs. 4C and 5I), suggesting an intrusive origin for the QzLD-B. Finally, quartz-rich breccias are not uniquely found at the ENSZ, but also along out-of-sequence breaching thrusts that place the Ermita and Alba formations on top of the Láncara Fm., north of Crémenes, and along thrusts placing Alba Fm. over Barcaliente Fm. in the underlying Pico Jano duplex, for which the EBSZ acted as a roof thrust (Figs. 1B, 4E and 11; Alonso, 1987b).

Several injection phases occurred locally, as evidenced by sand-rich dykes crosscutting earlier sand-rich breccias (Figs. 4D and 5K, Supplementary Figure 3), but most of the observed dyke–sill interconnected networks display a continuity that suggests a single emplacement episode at the outcrop scale. The lateral continuity of the basal quartz-rich breccias and their uniformity in fragment facies and quartz grains suggest that they were formed as a result of a limited amount of injections that mobilized large sand volumes.

Taking into account these observations, we regard the large-scale injection of quartz-sand grains as a late event in the displacement history of the Esla Nappe (Fig. 10C). Nonetheless, a small unquantified displacement along the thrust ensued the event, as evidenced by feeder dykes truncated by the ENSZ (Fig. 8B). This displacement could result from flexural slip accommodated in the ENSZ in relation to the tightening of folds during the subsequent evolution of the Esla Unit (Alonso, 1989).

7.5. Possible causes for sand injection

The cause for the achievement of large fluid overpressures in the footwall leading to the injections is unknown, but some hypothesis may be proposed. Stress fluctuations associated with the seismic cycle have been invoked as the cause for cyclic hydrofracturing and injection of sand at the ENSZ (Arboleya et al., 1999). However, there are no definite evidence that allow to demonstrate a seismic origin. Structures typically attributed to coseismic slip in carbonate rocks, such as sharp, narrow (*i.e.* a few mm) and continuous shear localization bands and well-defined slip surfaces truncating earlier structures (*e.g.* mirror-like surfaces, Fondriest et al., 2015; De Paola et al. 2015; Pozzi et al., 2018), or clearly fluidized cataclasites and ultracataclasites (Smith et al., 2011; Smeraglia et al., 2017) are lacking in the fault rocks of the Esla Nappe. Rather, strain has been largely localized into limestone cataclasites and ultracataclasites with a penetrative planar fabric. However, seismic structures are very likely to be obliterated and destroyed during subsequent deformation accommodated in the fault rocks (*e.g.* Wojtal and Mitra, 1988; Pozzi et al., 2018), and thus their absence is not conclusive regarding the possibility of seismic slip acting along the ENSZ. The static shear strength of the loose sandstones present in the footwall during Esla Nappe emplacement was likely largely reduced by the inferred high pore fluid pressures responsible for the injections, due to a low effective normal stress. Thus, even at a large depth, the sandstones may have been susceptible to cyclic loading caused by seismic shear waves produced either at the ENSZ or a different structure. However, under the same conditions of high pore fluid pressure, cohesionless or poorly cohesive granular sediments can become liquefied even without the need for a trigger (static liquefaction of Allen, 1982). Thus, in those conditions, it is difficult to prove a seismic trigger, and our evidence is inconclusive in that respect.

Thermal pressurization of fluids may cause fluid overpressures that lead to dynamic fault weakening during coseismic slip (Andrews, 2002; De Paola et al., 2011), but the pressurization is restricted to a few centimetres at the most within the slipping zone (Rice, 2006). Clearly, this process cannot be invoked as the source for the large volumes of pressurised fluid in the footwall of the Esla Nappe that led to the injections.

Other processes, such as the ones outlined in section 7.1 (tectonic loading, clay dehydration and solution-related pore closure), were potentially capable of generating a progressive fluid pressure increase in the footwall of the Esla Nappe, leading to large overpressures provided that there were lithologies above with sufficiently low permeability, such as the Alba Fm. and the LQz-U. The Alba Fm., a *ca.* 20 m-thick mudstone and marl sequence, may have acted as an impermeable barrier to fluid flow during the early stages of nappe emplacement (Arboleya, 1989). However, after *ca.* 6 km displacement the original footwall ramp was broken, with a new detachment horizon developing at the base of the Alba Fm. ahead of the branch line that eventually resulted in the development of the Pico Jano duplex (Alonso, 1987b). The Portilla, Ermita and Nocedo fms. came progressively into direct contact with the Láncara Fm. of the hangingwall, as the branch line migrated towards the foreland and the Alba Fm. was scrapped from their top. Nonetheless, as the upper portion of the Ermita and Portilla fms. were progressively comminuted, a thin low-permeability layer of quartz-bearing ultracataclasites was formed which acted as a new barrier to vertical fluid flow, maintaining the high fluid overpressures in the footwall (LQz-U). Rocks of similar composition and grain size have been shown to be characterised by low permeabilities capable of maintaining fluid overpressures over geological timescales (Mallon et al., 2005; Agosta et al., 2007).

At high fluid pressures, with the quartz grains in the footwall liquefied or at the verge of liquefaction, a catastrophic failure of the seal would have caused their fluidization and injection into the hangingwall. Failure occurred when the critical fluid overpressure needed to overcome the lithostatic normal stress acting across anisotropies of the hangingwall and the tensile strength of the material inside them was achieved (Delaney et al., 1986; Jolly and Sanderson, 1997). This could happen either by (i) increasing the fluid pressure in the footwall, or (ii) decreasing the normal stresses acting across anisotropies in the hangingwall.

Regarding the first possibility, fluid pressure could have increased progressively through the processes previously outlined, or more suddenly if a new fluid source fed the uppermost footwall. In the final stages of emplacement, the Esla Nappe and Pico Jano duplex were breached by out-of-sequence thrusts rooted in a mid-Devonian flat as a result of the transfer of displacement from the Láncara Fm. to the base

of the Portilla Fm. ahead of a broken footwall ramp (Fig. 1B; Alonso, 1987b). The breaching of the Portilla Fm. due to this late deformation could have created a hydraulic connection that transferred overpressured fluids from the underlying Huergas Fm. to the Upper Devonian formations. This could have provided an additional fluid source that caused fluid overpressure, leading to the injection process.

As for the second possibility, the transfer of displacement from the ENSZ to an underlying flat located near the base of the Portilla Fm (Fig. 1B). was likely associated with a modification of the stress regime in the ENSZ, so that it changed from simple shear to layer-parallel shortening, as frequently observed in foreland thrust sheets (*e.g.* Merle, 1998). During the activity of the ENSZ, the principal stress would have been oblique to the hangingwall flat bedding and the thrust surface, with an important resolved shear stress and a contribution of normal stress acting across these discontinuities (Fig. 12A; Sanderson, 1982; Merle, 1998, Teixell et al., 2000). Following the displacement transfer to an underlying flat, the principal compressive stress in the inactive ENSZ would become thrust- and bedding-parallel, decreasing the normal stress acting across these discontinuities, thus favouring their dilation and injection by fluidized quartz-sand sills and interconnecting dykes (Fig. 12B). Local vertical dilation and calcite vein precipitation in the weakest part of the ENSZ, the banded cataclasites and ultracataclasites of the footwall, can also be explained by this late variation in the stress regime (Figs. 5A and 6A&G).

Thrust-parallel compression could also result from the locking of the Esla Nappe due to unfavourable slip conditions, which in the end led to the transfer of displacement to the underlying Corniero and Valbuena nappes (Alonso, 1987b). During their emplacement, the ENSZ was also subjected to layer-parallel compression, also favouring thrust-normal dilation and potential injections.

8. Conclusions

Fault rock assemblages of the ENSZ record different deformation mechanisms and processes operating in the hangingwall and the footwall, owing to their rheology and fluid pressure conditions. Hangingwall lithologies, with the largest accumulated displacement, are competent limestones and dolostones that were deformed through cataclastic flow within a <50 cm-tick interval. The hangingwall-footwall intervening ultracataclasites deformed through localised cataclastic flow (20–40 cm layer) and pressure solution along dissolution seams, an interplay reflecting variations in the influx of fluid and fluid pressure conditions within these low-permeability fault rocks.

In the late stages of the Esla Nappe emplacement, a series of quartz sand-rich injection events caused intrusion fracturing in the base of the hangingwall, where a *ca.* 150 cm-thick basal interval of quartz-rich breccias was formed. Quartz-rich dykes and sills were injected along previously formed discontinuities and anisotropies such as thrust surfaces, bedding planes, joints and even stylolites, reaching structural heights up to 20 m above the base of the nappe. The injected slurry consisted of overpressured pore fluid, quartz-sand grains derived from the footwall and host-derived fragments.

The cause for the achievement of footwall fluid overpressures exceeding lithostatic values is currently unknown. Possible causes include fluid accumulation through clay dehydration reactions, tectonic loading, pore compaction, or fluid migration from underlying overpressured formations. While a seismic trigger responsible for the injection cannot be ruled out, the absence of extreme shear localization structures, such as principal slip surfaces, suggests that the process was related to progressive fluid accumulation in the footwall and to a late re-orientation of the stress regime acting on the ENSZ during the subsequent evolution of the Esla Unit.

Declaration of competing interest

The authors declare that they have no known competing financial interests or personal relationships that could have appeared to influence the work reported in this paper.

Acknowledgements

This work was supported by the Ministry of Economy and Competitiveness of Spain (MINECO) through the research projects (CATACRUSTAL, MINECO-15-CGL2014-53388-P) and (PETROCANTÁBRICA, MINECO-18-CGL2017-86487-P), and by the Govern-

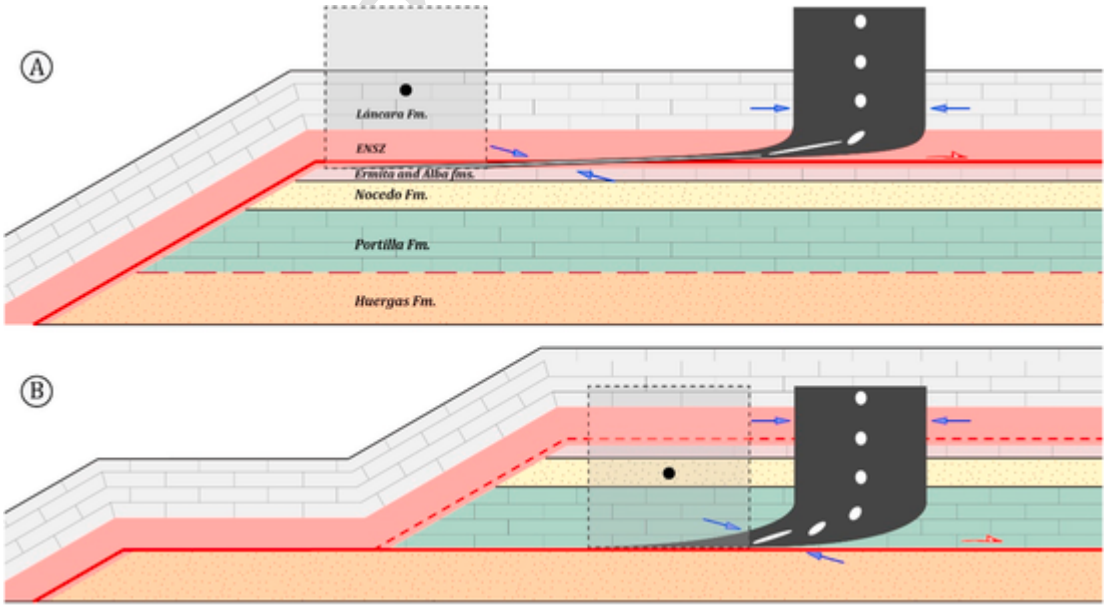

Fig. 12. Stress regime and finite strain markers associated with two distinct stages in the evolution of the Esla Nappe. Strain is exemplified by a square and internal ellipsoids. Maximum compressive stress is indicated with blue arrows. Note that the figure is not to scale, and the strain ellipsoid is a simplification: no continuous deformation is implied. (A) During the activity of the ENSZ, the base of the nappe was subjected to layer-oblique contraction. (B) During the development of a later thrust at the base of the Portilla Fm., the inactive ENSZ was subjected to layer-parallel contraction and associated vertical dilation, conditions that would favour sand injection along bedding-parallel sills and interconnecting dykes. (For interpretation of the references to colour in this figure legend, the reader is referred to the Web version of this article.)

ment of Asturias and FEDER funds through the research project (GEO-TEC, FC-GRUPIN-IDI/2018/000216). M.I. de Paz-Álvarez acknowledges a pre-doctoral contract from the FPU program of the Ministry of Education of Spain. Luis Pedro Fernández is thanked for discussions regarding sandstone lithification processes. The personnel of the Scientific Services of the University of Oviedo is thanked for thin section preparation and polishing, XRD analysis, and SEM guidance. We would also like to thank the editor Ian Alsop, Giacomo Pozzi and an anonymous referee for their constructive reviews and recommendations.

Appendix A. Supplementary data

Supplementary data to this article can be found online at https://doi.org/10.1016/j.jsg.2020.104230.

Summary of modifications

In this document an outline of the changes made with respect to the original manuscript is provided. Two versions of the revised manuscript have been uploaded: one with the tracking of the changes made, including responses to reviewer's comments, and another one where the changes have been fully incorporated into the text.

A point by point response to reviewer's comments is provided in a separate document.

- The text has been modified in some areas. Most notably, the geological setting of the Esla Nappe (section 2.2) has been slightly extended in order to outline the structural evolution of the Esla Nappe more clearly. Section 4.1 now includes the description of two more formations. Section 5 has been shortened by a 10%, but no major modifications have been made. Sections 7.1 and 7.5 have also been slightly modified in the light of the reviewer's comments. Terminology issues discussed by Reviewer 1 have been addressed where needed.
- Table 1 has been modified following the recommendation of Reviewer 2. It now includes a summary of the fault rock description, composition, fractal dimension, and interpretation of the fragment size distribution.
- Fig. 1 has been updated with the name of villages referred to in the manuscript.
- A new Fig. 2 has been produced with original orientation data of small scale structures from the base of the Esla Nappe, that allow an estimation of its transport sense independent from the literature.
- Scales and symbols in sample photographs of Figs. 4–6 and 8 have been increased in size and highlighted in order to improve their legibility.
- A new Fig. 10 contains three diagrams that schematically display the evolution of the fault rock assemblages of the ENSZ, following the suggestion of Reviewer 1.
- The location of photographs of Figs. 4–6 and 8 has been indicated in Fig. 11. Their structural context has been highlighted in the new Fig. 10.
- Supplementary material is provided following the recommendation of Reviewer 2. It consists of three additional figures. One of them (Sup. Fig. 2) contains more detailed photomicrographs of fault rock characteristics, whereas another one (Sup. Fig. 3) contains more field photographs of quartz-rich dykes and sills. Sup. Fig. 1 is a map identical to Fig. 11 with the location of the photographs in the supplementary figures.

References

Agosta, F., Prasad, M., Aydin, A., 2007. Physical properties of carbonate fault rocks, fucino basin (Central Italy): implications for fault seal in platform carbonates. Geofluids 7 (1), 19–32.

Allen, J.R.L., 1982. Sedimentary Structures: Their Character and Physical Basis. Elsevier, Amsterdam, p. 663.

Allmendinger, R.W., Cardozo, N., Fisher, D., 2012. Structural Geology Algorithms: Vectors and Tensors in Structural Geology. Cambridge University Press.

Alonso, J.L., 1987. Estructura y evolución tectonoestratigráfica de la Región del Manto del Esla (Zona Cantábrica, NW de España). Institución Fray Bernardino de Sahagún, Diputación Provincial de León.

Alonso, J.L., 1987. Sequences of thrusts and displacement transfer in the superposed duplexes of the Esla nappe region (cantabrian zone, NW Spain). J. Struct. Geol. 9 (8), 969–983.

Alonso, J.L., 1989. Fold reactivation involving angular unconformable sequences: theoretical analysis and natural examples from the Cantabrian Zone (Northwest Spain). Tectonophysics 170 (1–2), 57–77.

Alonso, J., Pulgar, J., García-Ramos, J., Barba, P., 1996. Tertiary basins and alpine tectonics in the cantabrian mountains (NW Spain). In: Friend, P.F., Dabrio, C.J. (Eds.), Tertiary Basins of Spain: the Stratigraphic Record of Crustal Kinematics. Cambridge University Press, pp. 214–227.

Alonso, J.L., Marcos, A., Suárez, A., 2009. Paleogeographic inversion resulting from large out of sequence breaching thrusts: the León fault (cantabrian zone, NW Iberia). A new picture of the external variscan thrust belt in the ibero-armorican arc. Geol. Acta 7, 451–473.

Andrews, D.J., 2002. A fault constitutive relation accounting for thermal pressurization of pore fluid. J. Geophys. Res.: Solid Earth 107 (B12) ESE-15.

Arboleya, M.L., 1981. La estructura del Manto del Esla (Cordillera Cantábrica, León). Bol. Geol. Min. 92 (1), 19–40.

Arboleya, M.L., 1983. Las rocas cataclásticas de la base del manto del Esla (Cordillera Cantábrica, León). Libro Jubilar J. M. Ríos, Tomo III. Instituto Geológico y Minero de España 157–163.

Arboleya, M.L., 1989. fault rocks of the Esla thrust (cantabrian mountains, N Spain) an example of foliated cataclasites. Ann. Tect. 3 (2), 99–109.

Arboleya, M.L., Julivert, M., Zamarreño, I., 1999. Datos sobre el mecanismo de emplazamiento del manto del Esla (Cordillera Cantábrica, NW de España) aportados por las rocas de falla. Trab. Geol. 21 (21), 47–61.

Barnett, W.P., Kurszlaukis, S., Tait, M., Dirks, P., 2011. Kimberlite wall-rock fragmentation processes: venetia K08 pipe development. Bull. Volcanol. 73 (8), 941–958.

Bethke, C.M., 1985. A numerical model of compaction-driven groundwater flow and heat transfer and its application to the paleohydrology of intracratonic sedimentary basins. J. Geophys. Res.: Solid Earth 90 (B8), 6817–6828.

Bjørlykke, K., 1988. Sandstone diagenesis in relation to preservation, destruction and creation of porosity. In: Chilingarian, G.V., Wolf, K.F. (Eds.), Developments in Sedimentology. In: Diagenesis, I), 41. Elsevier, pp. 555–588.

Blenkinsop, T.G., 1991. Cataclasis and processes of particle size reduction. Pure Appl. Geophys. 136 (1), 59–86.

Brooke, C.M., Trimble, T.J., Mackay, T.A., 1995. Mounded shallow gas sands from the Quaternary of the North Sea: analogues for the formation of sand mounds in deep water Tertiary sediments? Geological Society, London, Special Publications 94 (1), 95–101.

Burley, S.D., Kantorowicz, J.D., 1986. Thin section and SEM textural criteria for the recognition of cement-dissolution porosity in sandstones. Sedimentology 33 (4), 587–604.

Byrne, T., Fisher, D., 1990. Evidence for a weak and overpressured decollement beneath sediment-dominated accretionary prisms. J. Geophys. Res.: Solid Earth 95 (B6), 9081–9097.

Chi, G., Xue, C., Qing, H., Xue, W., Zhang, J., Sun, Y., 2012. Hydrodynamic analysis of clastic injection and hydraulic fracturing structures in the Jinding Zn-Pb deposit, Yunnan, China. Geoscience Frontiers 3 (1), 73–84.

Comte, P., 1959. Recherches sur les terrains anciens de la Cordillère Cantabrique. Memorias del Instituto Geológico y Minero de España, p. 60.

Cosgrove, J.W., 1995. The expression of hydraulic fracturing in rocks and sediments. Geological Society, London, Special Publications 92 (1), 187–196.

Delaney, P.T., Pollard, D.D., Ziony, J.I., McKee, E.H., 1986. Field relations between dikes and joints: emplacement processes and paleostress analysis. J. Geophys. Res.: Solid Earth 91 (B5), 4920–4938.

Demurtas, M., Smith, S.A., Prior, D.J., Spagnuolo, E., Di Toro, G., 2019. Development of crystallographic preferred orientation during cataclasis in low-temperature carbonate fault gouge. J. Struct. Geol. 126, 37–50.

De Paola, N., Hirose, T., Mitchell, T., Di Toro, G., Viti, C., Shimamoto, T., 2011. Fault lubrication and earthquake propagation in thermally unstable rocks. Geology 39 (1), 35–38.

De Paola, N., Holdsworth, R.E., Viti, C., Collettini, C., Bullock, R., 2015. Can grain size sensitive flow lubricate faults during the initial stages of earthquake propagation? Earth Planet Sci. Lett. 431, 48–58.

de Sitter, L.U., 1959. The río Esla nappe in the zone of León of the Asturian cantabric mountain chain. Notas Comunicaciones del Inst. Geol. Min. Espana 56, 3–24.

DiTullio, L., Byrne, T., 1990. Deformation paths in the shallow levels of an accretionary prism: the Eocene Shimanto belt of southwest Japan. Geol. Soc. Am. Bull. 102 (10), 1420–1438.

Duranti, D., Hurst, A., 2004. Fluidization and injection in the deep-water sandstones of the eocene Alba formation (UK north sea). Sedimentology 51 (3), 503–529.

Duranti, D., 2007. Large-scale sand injection in the Paleogene of the North Sea: modeling of energy and flow velocities. In: Hurst, A., Cartwright, J. (Eds.), Sand Injectites: Implications for Hydrocarbon Exploration and Production, 87. AAPG Memoir, pp. 129–139.

Fagereng, Å., 2013. On stress and strain in a continuous-discontinuous shear zone undergoing simple shear and volume loss. J. Struct. Geol. 50, 44–53.

Fondriest, M., Aretusini, S., Di Toro, G., Smith, S.A., 2015. Fracturing and rock pulverization along an exhumed seismogenic fault zone in dolostones: the Foiana Fault Zone (Southern Alps, Italy). Tectonophysics 654, 56–74.

Gutiérrez-Alonso, G., Fernández-Suárez, J., Weil, A.B., 2004. Orocline triggered lithospheric delamination. In: Sussman, A.J., Weil, A.B. (Eds.), Orogenic Curvature: Integrating Paleomagnetic and Structural Analyses, 383. GSA Special Paper, pp. 121–130.

Heilbronner, R., Keulen, N., 2006. Grain size and grain shape analysis of fault rocks. Tectonophysics 427 (1–4), 199–216.

Helset, H.M., Lander, R.H., Matthews, J.C., Reemst, P., Bonnell, L.M., Frette, I., 2002. The role of diagenesis in the formation of fluid overpressures in clastic rocks. In: Koestler, A.G., Hunsdale, R. (Eds.), Hydrocarbon Seal Quantification, 11. Norwegian Petroleum Society Special Publications, pp. 37–50.

Hurst, A., Scott, A., Vigorito, M., 2011. Physical characteristics of sand injectites. Earth Sci. Rev. 106 (3–4), 215–246.

Jébrak, M., 1997. Hydrothermal breccias in vein-type ore deposits: a review of mechanisms, morphology and size distribution. Ore Geol. Rev. 12 (3), 111–134.

Jolly, R.J., Sanderson, D.J., 1997. A Mohr circle construction for the opening of a pre-existing fracture. J. Struct. Geol. 19 (6), 887–892.

Jolly, R.J., Lonergan, L., 2002. Mechanisms and controls on the formation of sand intrusions. J. Geol. Soc. 159 (5), 605–617.

Jonk, R., 2010. Sand-rich injectites in the context of short-lived and long-lived fluid flow. Basin Res. 22 (4), 603–621.

Julivert, M., Marcos, A., 1973. Superimposed folding under flexural conditions in the cantabrian zone (hercynian cordillera, northwest Spain). Am. J. Sci. 273 (5), 353–375.

Kennedy, L.A., Logan, J.M., 1997. The role of veining and dissolution in the evolution of fine-grained mylonites: the McConnell thrust, Alberta. J. Struct. Geol. 19 (6), 785–797.

Labaume, P., 1987. Syn-diagenetic deformation of a turbiditic succession related to submarine gravity nappe emplacement, Autapie Nappe, French Alps. Geological Society, London, Special Publications 29 (1), 147–163.

Llana-Fúnez, S., Marcos, A., 2007. Convergence in a thermally softened thick crust: Variscan intracontinental tectonics in Iberian plate rocks. Terra. Nova 19 (6), 393–400.

Llana-Fúnez, S., Wheeler, J., Faulkner, D.R., 2012. Metamorphic reaction rate controlled by fluid pressure not confining pressure: implications of dehydration experiments with gypsum. Contrib. Mineral. Petrol. 164, 69–79.

Mallon, A.J., Swarbrick, R.E., Katsube, T.J., 2005. Permeability of fine-grained rocks: new evidence from chalks. Geology 33 (1), 21–24.

Maltman, A., 1994. Introduction and overview. In: Maltman, A. (Ed.), The Geological Deformation of Sediments. Chapman and Hall, Oxford, pp. 1–34.

Mandl, G., 1999. Faulting in Brittle Rocks: an Introduction to the Mechanics of Tectonic Faults. Springer Verlag, Berlin.

Mann, D.M., Mackenzie, A.S., 1990. Prediction of pore fluid pressures in sedimentary basins. Mar. Petrol. Geol. 7 (1), 55–65.

Matte, P., 1986. Tectonics and plate tectonics model for the Variscan belt of Europe. Tectonophysics 126 (2–4), 329–374.

Merino-Tomé, O., Suárez, A., Alonso, J.L., 2014. Mapa digital continuo E: 1:50000, Zona Cantábrica (zona-1000). GEODE, Mapa Geológico Digital Continuo de España (online). Available at:. http://info.igme.es/cartografiadigital/geologica/geodezona.aspx?Id=Z1000.

Merle, O., 1998. In: Emplacement Mechanisms of Nappes and Thrust Sheets, 9. Springer Science & Business Media.

Molenaar, N., de Jong, A.F.M., 1987. Authigenic quartz and albite in Devonian limestones: origin and significance. Sedimentology 34 (4), 623–640.

Murrell, S.A.F., Ismail, I.A.H., 1976. The effect of decomposition of hydrous minerals on the mechanical properties of rocks at high pressures and temperatures. Tectonophysics 31, 207–258.

Oliveira, J.T., González-Clavijo, E., Alonso, J.L., Armendáriz, M., Bahamonde, J.R., Braid, J.A., Colmenero, J.R., Dias da Silva, I., Fernandes, P., Fernández, L.P., Gabaldón, V., Jorge, R.S., Machado, G., Marcos, A., Merino-Tomé, O., Moreira, N., Murphy, J.B., Pinto de Jesus, A., Quesada, C., Rodrigues, B., Rosales, I., Sanz-López, J., Suárez, A., Villa, E., Piçarra, J.M., Pereira, Z., 2019. Synorogenic basins. In: Quesada, C., Oliveira, J.T. (Eds.), The Geology of Iberia: A Geodynamic Approach, ume 2. Springer, pp. 349–429.

Osborne, M.J., Swarbrick, R.E., 1997. Mechanisms for generating overpressure in sedimentary basins: a reevaluation. AAPG (Am. Assoc. Pet. Geol.) Bull. 81 (6), 1023–1041.

Palladino, G., Grippa, A., Bureau, D., Alsop, G.I., Hurst, A., 2016. Emplacement of sandstone intrusions during contractional tectonics. J. Struct. Geol. 89, 230–249.

Pérez-Estaún, A., Bastida, F., Alonso, J.L., Marquínez, J., Aller, J., Álvarez-Marrón, J., Marcos, A., Pulgar, J.A., 1988. A thin-skinned tectonic model for an arcuate fold and thrust belt: Cantabrian Zone (Variscan Ibero-Armorican Arc). Tectonics 7 (3), 517–537.

Phillips, C.A., Alsop, G.I., 2000. Post-tectonic clastic dykes in the Dalradian of Scotland and Ireland: implications for delayed lithification and deformation of sediments. Geol. J. 35 (2), 99–110.

Pozzi, G., De Paola, N., Nielsen, S.B., Holdsworth, R.E., Bowen, L., 2018. A new interpretation for the nature and significance of mirror-like surfaces in experimental carbonate-hosted seismic faults. Geology 46 (7), 583–586.

Reijers, T.J.A., 1972. Facies and diagenesis of the devonian Portilla limestone formation between the river Esla and the embalse de la Luna, cantabrian mountains, Spain. Leidse Geol. Meded. 47 (2), 163–217.

Rice, J.R., 2006. Heating and weakening of faults during earthquake slip. J. Geophys. Res.: Solid Earth 111 (B5), 1–29.

Rowe, K.J., Rutter, E.H., 1990. Palaeostress estimation using calcite twinning: experimental calibration and application to nature. J. Struct. Geol. 12 (1), 1–17.

Rupke, J., 1965. The Esla nappe, cantabrian mountains (Spain). Leidse Geol. Meded. 32, 1–74.

Rutter, E.H., Maddock, R.H., Hall, S.H., White, S.H., 1986. Comparative microstructures of natural and experimentally produced clay-bearing fault gouges. Pure Appl. Geophys. 124 (1–2), 3–30.

Rutter, E.H., 1995. Experimental study of the influence of stress, temperature, and strain on the dynamic recrystallization of Carrara marble. Journal of Geophysical Research, Solid Earth 100 (B12), 24651–24663.

Sammis, C.G., King, G.C., Biegel, R., 1987. The kinematics of gouge deformation. Pure Appl. Geophys. 125 (5), 777–812.

Sammis, C.G., King, G.C., 2007. Mechanical origin of power law scaling in fault zone rock. Geophys. Res. Lett. 34 (4) L04312, 1-4.

Sanderson, D.J., 1982. Models of strain variation in nappes and thrust sheets: a review. Tectonophysics 88 (3–4), 201–233.

Sibson, R.H., 1990. Conditions for fault-valve behaviour. Geological Society, London, Special Publications 54 (1), 15–28.

Smeraglia, L., Bettucci, A., Billi, A., Carminati, E., Cavallo, A., Di Toro, G., Natali, M., Passeri, D., Rossi, M., Spagnuolo, E., 2017. Microstructural evidence for seismic and aseismic slips along clay-bearing, carbonate faults. J. Geophys. Res.: Solid Earth 122 (5), 3895–3915.

Smith, S.A., Billi, A., Di Toro, G., Spiess, R., 2011. Principal slip zones in limestone: microstructural characterization and implications for the seismic cycle (Tre Monti Fault, Central Apennines, Italy). Pure Appl. Geophys. 168 (12), 2365–2393.

Storti, F., Billi, A., Salvini, F., 2003. Particle size distributions in natural carbonate fault rocks: insights for non-self-similar cataclasis. Earth Planet Sci. Lett. 206 (1–2), 173–186.

Swennen, R., Dewit, J., Fierens, E., Muchez, P., Shah, M., Nader, F., Hunt, D., 2012. Multiple dolomitization events along the pozalagua fault (pozalagua quarry, Basque–cantabrian basin, northern Spain). Sedimentology 59 (4), 1345–1374.

ten Haaf, E., 1959. Graded Beds of the Northern Apennines PhD thesis. (Rijksuniversiteit te Groningen).

Taylor, B.J., 1982. Sedimentary dykes, pipes and related structures in the Mesozoic sediments of south-eastern Alexander Island. Br. Antarct. Surv. Bull. 51, 1–42.

Teixell, A., Durney, D.W., Arboleya, M.L., 2000. Stress and fluid control on decollement within competent limestone. J. Struct. Geol. 22 (3), 349–371.

Tesei, T., Collettini, C., Viti, C., Barchi, M.R., 2013. Fault architecture and deformation mechanisms in exhumed analogues of seismogenic carbonate-bearing thrusts. J. Struct. Geol. 55, 167–181.

Tesei, T., Collettini, C., Barchi, M.R., Carpenter, B.M., Di Stefano, G., 2014. Heterogeneous strength and fault zone complexity of carbonate-bearing thrusts with possible implications for seismicity. Earth Planet Sci. Lett. 408, 307–318.

van Adrichem Boogaert, H.A., 1967. Devonian and lower carboniferous conodonts of the cantabrian mountains (Spain) and their stratigraphic application. Leidse Geol. Meded. 39, 129–192.

van der Meer Mohr, C.G., 1969. The stratigraphy of the cambrian lancara formation between the luna river and the Esla river in the cantabrian mountains, Spain. Leidse Geol. Meded. 43, 233–316.

van Loevezijn, G.B.S., 1986. Stratigraphy and facies of the Nocedo, fueyo and Ermita formations (upper devonian to lowermost carboniferous) in León, N Spain. Scripta Geol. 81, 1–116.

Vigorito, M., Hurst, A., 2010. Regional sand injectite architecture as a record of pore-pressure evolution and sand redistribution in the shallow crust: insights from the Panoche Giant Injection Complex, California. J. Geol. Soc. 167 (5), 889–904.

Winslow, M.A., 1983. Clastic dike swarms and the structural evolution of the foreland fold and thrust belt of the southern Andes. Geol. Soc. Am. Bull. 94 (9), 1073–1080.

Wojtal, S., Mitra, G., 1986. Strain hardening and strain softening in fault zones from foreland thrusts. Geol. Soc. Am. Bull. 97 (6), 674–687.

Wojtal, S., Mitra, G., 1988. Nature of deformation in some fault rocks from Appalachian thrusts. Geol. Soc. Am. Spec. Pap. 222, 17–33.